A&A 476, 99–119 (2007)
DOI: 10.1051/0004-6361:20077918

Astronomy & Astrophysics

Radio morphology and spectral analysis of cD galaxies in rich and poor galaxy clusters

S. Giacintucci[1,2,3], T. Venturi[1], M. Murgia[1,4], D. Dallacasa[1,3], R. Athreya[5], S. Bardelli[2], P. Mazzotta[6,7], and D. J. Saikia[5]

[1] INAF – Istituto di Radioastronomia, via Gobetti 101, 40129 Bologna, Italy
e-mail: tventuri@ira.inaf.it
[2] INAF – Osservatorio Astronomico di Bologna, via Ranzani 1, 40126 Bologna, Italy
[3] Dipartimento di Astronomia, Università di Bologna, via Ranzani 1, 40126 Bologna, Italy
[4] INAF – Osservatorio Astronomico di Cagliari, Loc. Poggio dei Pini, Strada 54, 09012 Capoterra, Italy
[5] Tata Institute of Fundamental Research, National Centre for Radio Astrophysics, Ganeshkhind, Pune 411 007, India
[6] Dipartimento di Fisica, Universitá di Roma Tor Vergata, via della Ricerca Scientifica 1, 00133 Roma, Italy
[7] Harvard-Smithsonian Centre for Astrophysics, 60 Garden Street, Cambridge, MA 02138, USA

Received 21 May 2007 / Accepted 21 August 2007

ABSTRACT

Aims. We present a radio morphological study and spectral analysis of a sample of 13 cD galaxies in rich and poor clusters of galaxies.
Methods. Our study is based on new high sensitivity Giant Metrewave Radio Telescope (GMRT) observations at 1.28 GHz, 610 MHz and 235 MHz, and on archival data. From a statistical sample of cluster cD galaxies we selected those sources with little information available in the literature and promising for the detection of aged radio emission. As well as the high sensitivity images for all 13 radio galaxies, we present also a detailed spectral analysis for 7 of them.
Results. We found a variety of morphologies and linear sizes, as typical for radio galaxies in the radio power range sampled here (low to intermediate power radio galaxies). The spectral analysis shows that 10/13 radio galaxies have a steep radio spectrum, with spectral index $\alpha \geq 1$. In general, the radiative ages and growth velocities are consistent with previous findings that the evolution of radio galaxies at cluster centres is affected by the dense external medium (i.e. low growth velocities and old ages). We suggest that the dominant galaxies in A 2622 and MKW 03s are dying radio sources, which at present are not fed by nuclear activity. On the other hand, the spectacular source at the centre of A 2372 might be a very interesting example of a restarted radio galaxy. For this source we estimated a life cycle of the order of 10^6 yr.

Key words. radio continuum: galaxies – galaxies: clusters: general

1. Introduction

Nuclear radio emission associated with elliptical galaxies, i.e. the *radio galaxy phenomenon*, is one of the most studied phenomena in radio astronomy. Among ellipticals, cluster dominant cD galaxies (Mathews et al. 1964) are the most extreme and interesting population, as they are among the most luminous and massive galaxies known. They are found at the centre of the potential wells of both rich and poor clusters of galaxies, and they are usually located at the peak of the cluster X-ray emission (Jones et al. 1979).

Despite the large amount of data available for this class of radio sources, some basic questions related to their birth, evolution and death have no answer yet. For example, it is still not known what triggers radio emission in elliptical galaxies, and what the role of the large- and small-scale environment is. The presence of a central massive black hole accreting material is crucial, but it is not the only requirement, since it is widely accepted that massive and supermassive black holes are hosted in radio quiet sources as well (Merritt & Ferrarese 2001).

The accumulating evidence for recurrent radio activity in elliptical galaxies suggests that all ellipticals may alternate phases of radio activity and quiescence (i.e. Lara et al. 1999; Giovannini et al. 1998; Schoenmakers et al. 2000), however the cause of such intermittent activity and the duty cycle of the radio emission are still unknown.

In recent years, thanks to the high-resolution X-ray images from the satellites *Chandra* and XMM–Newton, it has become clear that major feedback processes take place in the central regions of galaxy clusters and groups, between the AGN activity of the dominant galaxy and the intracluster gas (for recent literature on the subject see Böhringer et al. 2007). The relativistic plasma of the central radio galaxies may interact with the ICM, displacing the X-ray emitting gas and creating depressions in the X-ray surface brightness, referred to as *holes*, *cavities* or *bubbles* (see for instance the review by Blanton 2004). Such cavities may be filled with radio emission from the lobes of the central AGN (*radio-filled cavities*, e.g. Hydra A, McNamara et al. 2000; Perseus, Fabian et al. 2000; A 2052, Blanton et al. 2001; MKW 03s, Mazzotta et al. 2004). In other cases an offset is found between radio lobes and cavities (*ghost cavities*, e.g. Perseus, Fabian et al. 2000; A 2597, McNamara et al. 2001). Both types of cavities may be present in the same cluster (like Perseus), suggesting that repeated outbursts of radio activity of

Table 1. Rich Abell and poor cluster cDs.

Cluster name	$R^{(\diamond)}$	Galaxy name h,m,s	RA_{J2000} °, ′, ″	Dec_{J2000}	z (mJy)	$S_{1.4\ GHz}$ (W Hz^{-1})	$\log P_{1.4\ GHz}$
Rich Abell clusters							
A 1663	1	2MASX J1302−0230	13 02 52.6	−02 30 59	0.0847	39	23.84
A 1775$^{(*)}$	2	UGC 08669 (1)	13 41 49.1	+26 22 25	0.0757	24	23.52
		UGC 08669 (2)	13 41 50.4	+26 22 13	0.0734	298	24.71
A 2162	0	NGC 6086	16 12 35.6	+29 29 04	0.0319	111	23.40
A 2372	0	2MASX J2145−1959	21 45 15.5	−19 59 41	0.0587	417	24.53
A 2480	1	2MASX J2245−1737	22 45 59.0	−17 37 33	0.0684	406	24.66
A 2622	0	2MASX J2335+2722	23 35 01.5	+27 22 20	0.0613	78	23.84
Poor clusters							
MKW 01s		UGC 04956	09 20 02.2	+01 02 18	0.0172	11	21.86
MKW 01		NGC 3090	10 00 30.2	−02 58 06	0.0203	25	22.37
MKW 02		CGCG 009−062	10 30 10.6	−03 09 49	0.0380	385	24.11
MKW 06		CGCG 018−111	14 17 36.5	+02 03 18	0.0530	42	23.44
MKW 07		UGC 09371	14 33 59.1	+03 46 41	0.0302	94	23.28
MKW 03s		NGC 5920	15 21 51.8	+07 42 32	0.0453	105	23.72
AWM 05		NGC 6269	16 57 58.1	+27 51 16	0.0348	51	23.15

$^{(*)}$ This cluster hosts a dumb-bell system at its centre; the 1.4 GHz flux densities given for the two radio galaxies are from the FIRST survey.
$^{(\diamond)}$ Richness class R, defined by Abell (e.g. ACO catalogue of rich galaxy clusters, Abell et al. 1989), on the basis of the number of galaxies in the magnitude range $[m_3; m_3 + 2]$.

the central galaxy could play a role in the formation of the holes, the ghost cavities being the result of a previous AGN burst (McNamara et al. 2001) moved outwards by buoyancy. The central regions of galaxy clusters and groups are thus expected to be very promising for the study of aged radio galaxies, for recurrent activity, and for our understanding of the birth and evolution of radio galaxies.

In order to study the morphological and spectral properties of dominant cluster galaxies in the radio band, and to address the question of their age and evolution, in this paper we present new radio observations carried out with the Giant Metrewave Radio Telescope (GMRT, Pune, India) at 1.28 GHz, 610 MHz and 235 MHz for a sample of 13 cD galaxies located at the centre of rich clusters and poor groups. The sources belong to a large statistical sample of 132 cD galaxies we selected in order to investigate the properties of this class of radio sources and to understand how the external environment may influence them.

The paper is organised as follows: in Sect. 2 we report on the sample selection and on the list of clusters observed with the GMRT; in Sect. 3 we describe the observations and the data reduction; the radio images and the spectral analysis are given in Sects. 4 and 5 respectively; our results are discussed in Sect. 6 and a brief summary is given in Sect. 7. In the Appendix we present the 235 MHz image of the cD galaxy in A 2634, which is located within the GMRT field of view of one of the cluster presented in this paper. A 2634 belongs to our complete sample of cD galaxies, but it was not selected as a target for the GMRT observations, given the amount of radio data available for this cluster in the literature.

In this paper we adopt the ΛCDM cosmology, with $H_0 = 70\ km\ s^{-1}\ Mpc^{-1}$, $\Omega_m = 0.3$ and $\Omega_\Lambda = 0.7$. The spectral index α is defined according to $S \propto \nu^{-\alpha}$.

2. The sample of cluster cD galaxies

We report here the most relevant information on the compilation of our statistical sample of 132 cD galaxies in rich and poor clusters, selected through a comprenhensive study of their radio properties (work in progress). The sample includes the 109 Abell clusters from the Struble & Rood (1987) morphological catalogue and from the cD galaxy sample in Valentjin & Bijleveld (1983) with $Dec_{J2000} > -30°$ and redshift $z \leq 0.1$[1], optically classified as cD clusters. From Valentjin & Bijleveld (1983) we further selected 23 poor clusters hosting a cD, with the same declination and redshift constraints. The poor cluster cDs belong to the MKW sample (Morgan et al. 1975) and to the AWM sample (Albert et al. 1977).

Our selection was carried out on the basis of the optical information only, therefore no a priori knowledge of the radio properties of the cDs and the X-ray properties of the hosting clusters was considered.

We searched for information on the radio emission for all the cD galaxies in our sample by inspection of the 1.4 GHz NVSS (Condon et al. 1998) and FIRST (Becker et al. 1995) surveys, and from the literature. We found that ∼60% of the cDs in the sample are radio loud above the NVSS sensitivity limit, at levels from a few mJy to ∼Jy. On the basis of the radio information available in the literature, we selected all clusters still lacking high sensitivity and high resolution data at 1.4 GHz (beyond the NVSS and FIRST images), and a number of clusters that appeared promising for the search of aged radio emission related to a previous burst of activity of the central galaxy. Our final list includes a total of 13 objects (in both rich and poor clusters) given in Table 1. The columns in the table provide the following information: cluster name; cluster richness (available for the Abell clusters only); cD galaxy name; J2000 optical coordinates of the cD; cluster redshift; 1.4 GHz flux density measured on the NVSS image, and corresponding radio power at the redshift of the optical galaxy.

3. Radio observations and data reduction

The observations were carried out with the GMRT at 1.28 GHz, 610 and 235 MHz. In particular, 1.28 GHz observations were carried out for 8 of the 13 galaxies in our sample still lacking high sensitivity and high resolution observations at this

[1] We used the NASA/IPAC Extragalactic Database NED to obtain updated (although inhomogenous) redshift information for all the clusters.

Table 2. GMRT observations.

Cluster	Obs. date	Obs. Freq. MHz	$\Delta\nu$ MHz	Obs. time min	Beam, PA $''\times''$, $^\circ$	rms mJy b^{-1}
A 1663	Aug. 2003	1280	32	60	3.0×2.1, 17	0.015
A 1775	Aug. 2003	610	16	45	5.1×3.9, 49	0.130
	Jul. 2005	235	8	100	12.7×9.1, 63	1.500
A 2162	Aug. 2003	610	16	60	7.1×4.9, –83	0.150
	Jul. 2005	235	8	50	14.7×10.8, –85	1.000
A 2372	Jul. 2005	610	32	160	7.5×5.7, 38	0.065
	Jul. 2005	235	8	160	19.7×13.8, –8	1.500
A 2480	Aug. 2003	1280	32	45	2.9×2.0, 13	0.030
A 2622	Jul. 2005	610	32	220	5.5×4.9, 89	0.050
	Jul. 2005	235	8	220	17.1×11.4, 53	0.800
MKW 01s	Aug. 2003	1280	32	60	3.5×2.3, 2	0.015
MKW 01	Aug. 2003	1280	32	60	3.1×2.1, 28	0.020
MKW 02	Aug. 2003	610	16	100	5.1×4.6, 42	0.130
	Jul. 2005	235	8	100	12.1×9.7, 65	0.650
MKW 06	Aug. 2003	1280	32	60	3.3×2.3, 45	0.020
MKW 07	Aug. 2003	1280	32	60	3.5×2.4, 49	0.030
	Aug. 2003	610	16	120	5.8×4.4, 57	0.100
	Jul. 2005	235	8	100	14.0×9.1, 50	1.500
MKW 03s	Aug. 2003	1280	32	60	3.0×2.5, –38	0.030
	Aug. 2003	610	16	90	5.4×4.5, 61	0.150
	Jul. 2005	235	8	90	12.1×9.1, 52	2.000
AWM 05	Aug. 2003	1280	32	60	3.2×2.6, –72	0.025

frequency, while observations at 610 MHz and 235 MHz were carried out for those sources (7/13) candidate for recurrent radio activity. For this reason, not all galaxies listed in Table 1 were observed at all three frequencies. The observation logs are reported in Table 2, where the following information is provided: cluster name; observing date; observed frequency; total frequency bandwidth (MHz); total time on source (minutes); half power bandwidth (*HPWB*) of the full array (arcsec × arcsec, position angle in degrees); rms level (1σ) in the full resolution image (mJy b^{-1}).

The 1.28 GHz observations were performed using both the upper and lower side band, for a total observing bandwidth of 32 MHz; the August 2003 610 MHz observations were carried out using the dual receiver 235/610 MHz, and have a bandwidth of 16 MHz. Since the 235 MHz band of those observations was affected by major interference which jeopardized the whole data reduction, those sources were reobserved at 235 MHz in July 2005 with a bandwidth of 8 MHz.

The data at all frequencies were collected in spectral-line mode (128 channels at 1.28 GHz and 610 MHz, and 64 channels at 235 MHz), with a spectral resolution of 125 kHz/channel. The data calibration and reduction were performed using the NRAO Astronomical Image Processing System (AIPS) package. An accurate editing was needed to identify and remove the data affected by radio frequency interference (RFI) at 235 MHz. In order to find a compromise between the size of the dataset and the need to minimize bandwidth smearing effects within the primary beam, after bandpass calibration the central channels in each individual dataset were averaged to 6 channels of ∼1 MHz each at 235 MHz and ∼2 MHz each at 610 MHz. At 1.28 GHz the central band was averaged to 1 single channel of ∼11 MHz.

In each step of the data reduction we used the wide-field imaging technique, and after a number of phase self-calibration cycles, we produced the final images for each cluster. The upper and lower side band datasets at each observing frequency were self–calibrated separately and then combined to produce the final images. The rms noise level (1σ) achieved in the final full resolution images is in the range 13−30 μJy at 1.28 GHz, 50−150 μJy at 610 MHz and 0.65−2 mJy at 235 MHz (see Table 2). The spread in the noise level depends mostly on the total time on source and residual RFI, especially at 235 MHz. Unless specified otherwise, the average residual amplitude errors in our data are of the order of $\lesssim$5% at all frequencies.

4. The radio images

In this section we present our new GMRT radio images of the clusters listed in Tables 1 and 2. In the presentation of the images we chose to group the sources according to the frequency of the observations, for a clearer reference to the information reported in the tables. We used the AIPS task JMFIT to measure the total flux density and angular size of the unresolved components, while the task TVSTAT was used to determine the total flux density of extended radio sources. Given the high signal-to-noise ratio in all our images, the error associated with the flux density measurement is dominated by the uncertainty in the residual amplitude calibration errors. The conversion factor from angular to linear scale is reported in the caption of each figure.

Where possible, we carried out a detailed study of the radio integrated spectrum, and/or spectral index images. This analysis is presented in Sect. 5.

4.1. Clusters observed at 1.28 GHz

We present the radio images of the clusters observed at 1.28 GHz only (Table 2). In Table 3 we summarize the most relevant observational properties of each source, i.e. the 1.28 GHz total flux density and largest linear size (LLS). In those cases where the source structure can be unambiguosly separated into a number of individual components, information is listed for each of them. A brief note for all sources is given below.

A 1663 – In Fig. 1 we present the GMRT 1.28 GHz full resolution contours of the source, superposed on the Sloan Digital Sky Survey (SDSS) optical image of the cD galaxy. At this resolution the source can be classified as triple, and extends on the galactic scale with linear size of $\approx 40 \times 16$ kpc. Between the two

Table 3. Radio source data at 1.28 GHz.

Cluster	component	$S_{1280\ \mathrm{MHz}}$ (mJy)	LLS kpc
A 1663	tot.	40	$\sim 40 \times 16$
	A	26	~ 16
	B	10	~ 16
	C	4	<3.5
A 2480	tot.	472	$\sim 35 \times 14$
MKW 01s	tot.	12	<0.02
MKW 01	tot.	30	~ 21
	C	23	<0.7
	H	7	~ 21
MKW 06	tot.	34	$\sim 165 \times 46$
	A	14	$\sim 23 \times 10$
	B	16	$\sim 57 \times 46$
	C	4	$\sim 52 \times 33$
AWM 05	tot.	50	$\sim 35 \times 9$
	A	30	$\sim 8 \times 5$
	B	10	$\sim 10 \times 9$
	C	10	$\sim 12 \times 8$

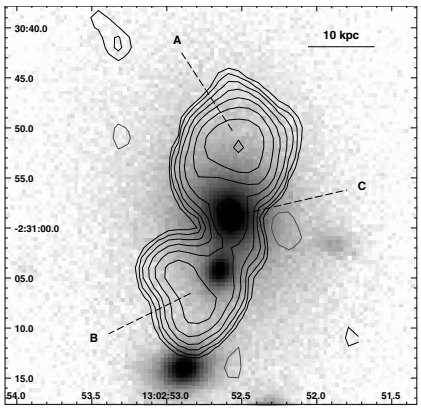

Fig. 1. A 1663 – GMRT 1.28 GHz radio contours of the central radio galaxy overlaid on the SDSS optical frame. Different source components are labelled A, B and C. The 1σ level in the image is 15 μJy b^{-1}. Logarithmic contours are reported, starting from ± 0.045 mJy b^{-1}. The contour peak flux is 13.53 mJy b^{-1}. The *HPWB* is $3.0'' \times 2.1''$, PA 17°. For this source $1'' = 1.59$ kpc.

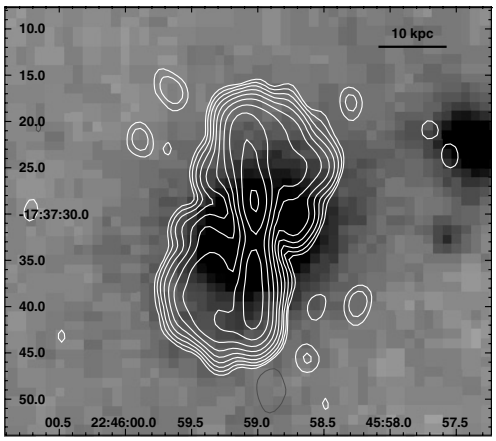

Fig. 2. A 2480 – GMRT 1.28 GHz radio contours of the central radio galaxy on the POSS–2 optical image. The 1σ level in the image is 30 μJy b^{-1}. Logarithmic contours are reported, starting from ± 0.09 mJy b^{-1}. The contour peak flux is 51.26 mJy b^{-1}. The *HPWB* is $2.9'' \times 2.0''$, PA 13°. For this source $1'' = 1.31$ kpc.

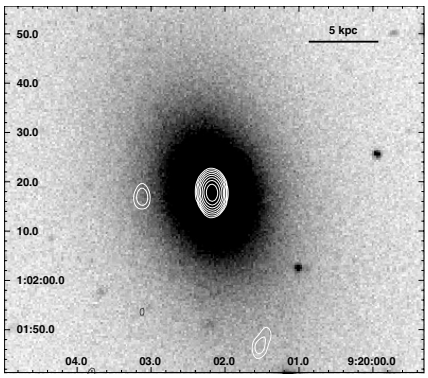

Fig. 3. MKW01s – GMRT 1.28 GHz radio contours of the central radio galaxy overlaid on the SDSS image. The 1σ level in the image is 15 μJy b^{-1}. Logarithmic contours are reported, starting from ± 0.045 mJy b^{-1}. The contour peak flux is 30.83 mJy b^{-1}. The *HPWB* is $3.5'' \times 2.3''$, PA 2°. For this source $1'' = 0.35$ kpc.

extended radio lobes (labelled A and B in Fig. 1), a third compact component (C) is detected at the location of the optical nucleus of the cD galaxy. No radio emission from the cD was detected with the VLA in the B array configuration at 4.7 GHz by Ball et al. (1993) at a sensitivity limit of 0.7 mJy.

The GMRT 1.28 GHz total flux density of the source (Table 3) is in good agreement with the 1.4 GHz value measured on the NVSS image (Table 1), despite the difference in angular resolution. The source radio power is typical of FR I sources (Fanaroff & Riley 1974), and consistent with its radio morphology.

A 2480 – The GMRT 1.28 GHz image is presented in Fig. 2. The cD galaxy in A 2480 hosts a double radio galaxy of galactic size ($\sim 35 \times 14$ kpc), with two jets and Z–shaped lobes. Our image is consistent with the VLA–B 4.7 GHz image published in Ball et al. (1993). Both the radio morhology and power are typical of a FR I/FR II transition source. It is the most powerful radio source among those presented in this paper.

A detailed study of the spectral properties for this object is given in 5.1.

MKW 01s – The GMRT 1.28 GHz full resolution image of the radio emission from the dominant galaxy in MKW 01s is shown in Fig. 3, superposed on the optical SDSS frame. At this frequency and resolution we detected a compact radio source with a flux density of 12 mJy (Table 3), in agreement with the value from the NVSS (Table 1) and FIRST images ($S_{1.4\ \mathrm{GHz}} = 11$ mJy). This source is the closest to us and the least powerful among those presented in this paper. A two dimensional Gaussian fit of the source provides a deconvolved linear size of $\sim 170 \times 140$ pc.

A 9 mJy unresolved radio source was also detected with the VLA at 1.45 GHz, with a resolution of $\sim 13''$, by Burns et al. (1987). A total flux density of 10 ± 3 mJy was measured at 2.38 GHz with the Arecibo telescope by Dressel & Condon (1978). Using this value a spectral index of $\alpha = 0.3 \pm 0.6$ is obtained between 1.28 GHz and 2.38 GHz.

The nature of this radio source is unclear. Its radio morphology, total power and unknown spectral shape make it difficult to discriminate between a compact low power AGN and a radio emission of nuclear starburst origin.

MKW 01 – The radio emission of the cD galaxy is reported in Fig. 4, where a full resolution and a tapered image are given in the left and right panel respectively. In both images the source is characterised by a compact bright component (labelled C in Fig. 4) surrounded by an amorphous low surface brightness

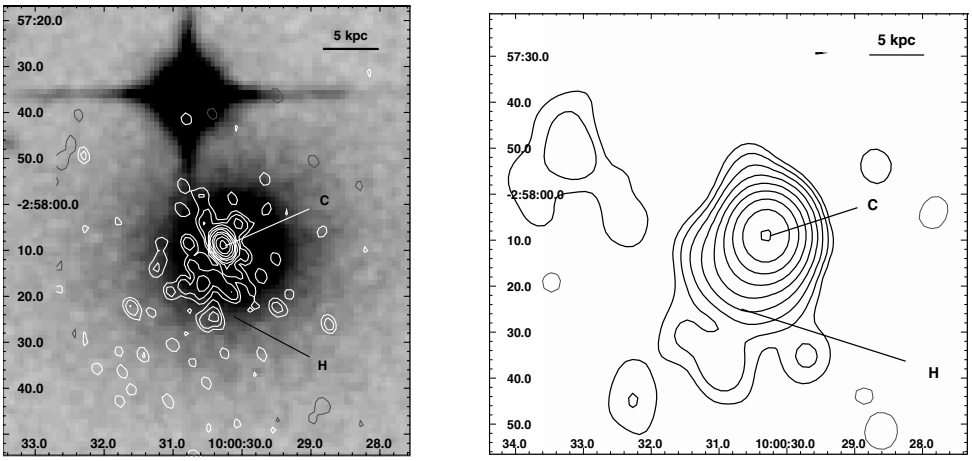

Fig. 4. MKW01 – GMRT 1.28 GHz full resolution (on the POSS–2 optical image, *left panel*) and u–v tapered low resolution (*right panel*) contours of the central radio galaxy. The 1σ level in the image is 20 μJy b^{-1} and 30 μJy b^{-1} respectively. Logarithmic contours are reported, starting from $\pm 3\sigma$. The contour peak flux is 22.9 mJy b^{-1} in the right panel and 24.4 mJy b^{-1} in the left panel. The *HPWB* is 3.1″ × 2.1″, PA 28° and 10.5″ × 9.6″, PA −6° respectively. In both panels letters C and H indicate the core and halo components of the source. For this source 1″ = 0.41 kpc.

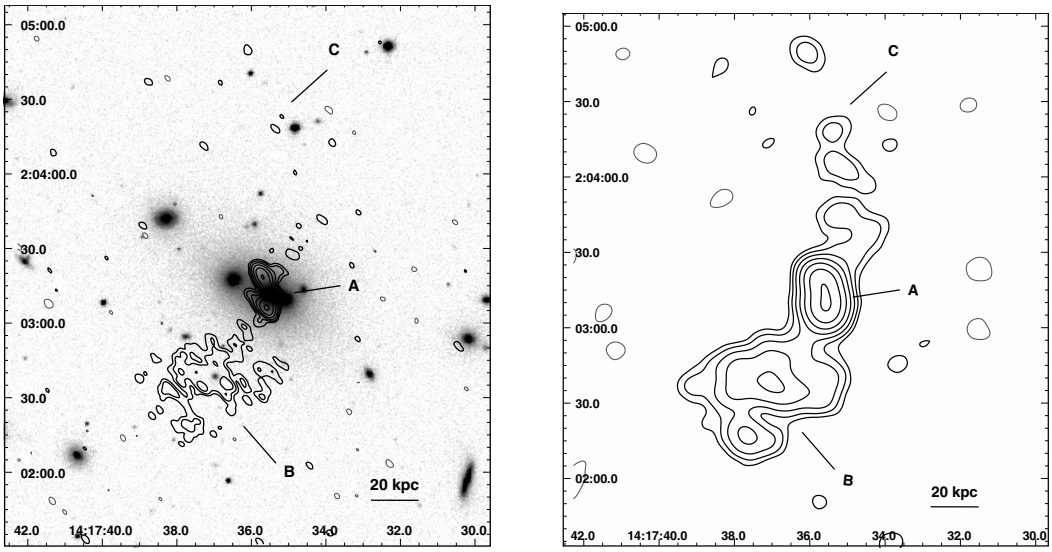

Fig. 5. MKW06 – GMRT 1.28 GHz full resolution (on SDSS optical image, *left panel*) and low resolution (*right panel*) of the central radio galaxy. The 1σ level in the image is 20 μJy b^{-1} and 25 μJy b^{-1} respectively. Logarithmic contours are reported, starting from $\pm 4\sigma$. The contour peak flux is 2.81 mJy b^{-1} and 7.00 mJy b^{-1} in left and right panels respectively. The *HPWB* is 5.4″ × 2.8″, PA 47° in the left panel, and 10.9″ × 8.9″, PA 62° in the right panel. Letters A, B and C indicate the source components. For this source 1″ = 1.03 kpc.

feature (H in the figure). This morphology is reminiscent of the core-halo radio sources found in a number of cool core clusters, for example 3C 317 (Venturi et al. 2004), 2A 0335+096 (Sarazin et al. 1995), and PKS 0745−191 (Baum & O'Dea 1991). In Table 3 we report the individual flux density values of components C and H. The flux density of C was estimated through a two dimensional Gaussian fit in the highest resolution image (Fig. 4, left panel). The fit provides a deconvolved size of ∼0.7 × 0.4 kpc. The halo emission extends over a scale of ∼21 kpc in the low resolution image, and it is completely embedded in the optical galaxy (Fig. 4, right panel).

Previous 1.45 GHz VLA observations (Burns et al. 1987) show only a compact component coincident with the cD galaxy in MKW 01. The flux density in that image (∼13″ resolution) is $S_{1.45\ \mathrm{GHz}}$ = 21.4 mJy. This value is consistent with the 1.4 GHz NVSS flux density reported in Table 1, and they are both ∼20% lower than our measurement at 1.28 GHz. Such a difference is significant, even if we account for spectral index effects, and might suggest variability of the central component associated with the nucleus of the cD galaxy.

No information is available in the literature at other frequencies, therefore no spectral study is possible for this source.

MKW 06 – The 1.28 GHz image of the source is presented in Fig. 5. The left panel shows the full resolution image overlaid on the SDSS optical frame: a radio galaxy of galactic size (∼23 × 10 kpc) is located at the position of the cD galaxy and is characterised by a double component (labelled as A in the figure). A region of low surface brightness emission, indicated as B in the figure, is detected South of A. In the low resolution image (right panel of Fig. 5) this region may be interpreted as the southern lobe of a double radio source, extending over ∼165 kpc, larger than the structure detected at high resolution. The northern lobe (labelled as C in the right panel of Fig. 5) has a very low surface brightness and is much fainter than the southern one. An image

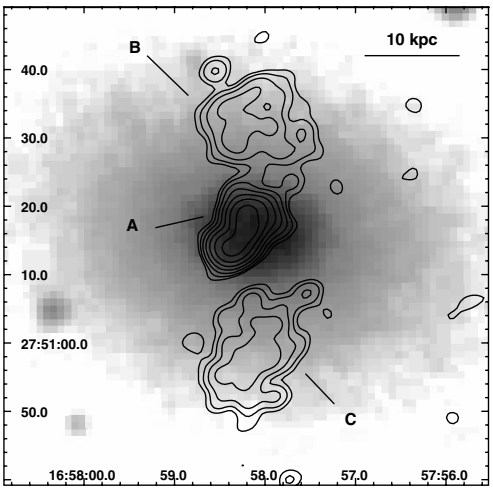

Fig. 6. AMW05 – GMRT 1.28 GHz radio contours of the central radio galaxy overlaid on the optical POSS–2 frame. The 1σ level in the image is 25 μJy b^{-1}. Logarithmic contours are reported, starting from $\pm$0.075 mJy b^{-1}. The contour peak flux is 8.29 mJy b^{-1}. The *HPWB* is $3.2'' \times 2.0''$, PA -72°. The source components are labelled as A, B and C. For this source $1'' = 0.69$ kpc.

Table 4. Radio source data at 235 and 610 MHz.

Cluster	component	$S_{235\ \mathrm{MHz}}$ (mJy)	$S_{610\ \mathrm{MHz}}$ (mJy)	$\alpha^{610\ \mathrm{MHz}}_{235\ \mathrm{MHz}} \pm 0.07$	LLS kpc
A 1775	tot.	2035	896	0.85	–
	D	135	62	0.82	$\sim 56 \times 21$
	HT	1900	834	0.86	$\sim 381 \times 56$
A 2162	tot.	218$^{(*)}$	240	0.10$^{(*)}$	$\sim 90 \times 38$
A 2372	tot	2657	1106	0.92	$\sim 842 \times 117$
	A	8	14	–0.59	$\sim 28 \times 15^{\circ}$
	B	1310	616	0.79	$\sim 260 \times 115$
	C	1410	476	0.92	$\sim 380 \times 100$
A 2622	tot.	1184	310	1.40	$\sim 180 \times 60$
	A	–	193	–	$\sim 32 \times 24^{\circ}$
	B	–	59	–	$\sim 47 \times 47^{\circ}$
	C	–	54	–	$\sim 47 \times 35^{\circ}$
MKW 02	tot.	1700	245	2.03	~ 670
	A	571	60	2.36	$\sim 135 \times 90$
	B	940	150	1.92	$\sim 180 \times 90$
	C	50	31	0.50	<2.1
	D	15	3	1.69	~ 23

* This value has large uncertainties due to problems with the secondary calibrator at 235 MHz.
$^{\circ}$ Values estimated from the full resolution 610 MHz image.

of this radio source was also reported in Burns et al. (1987), who classified it as a possible head-tail, but they did not exclude a double morphology, possibly lost due the limited sensitivity of their observations.

The 1.28 GHz total flux density of the source reported in Table 3 was measured on the low resolution image. It is in agreement with the Burns et al. (1987) measurement ($S_{1.5\ \mathrm{GHz}} = 33.9$ mJy), and it is slightly lower than the NVSS value (Table 1), probably due to the different angular resolution. Table 3 summarises the flux density and size of each component.

AWM 05 – In Fig. 6 we show the GMRT 1.28 GHz full resolution contours of the source, overlaid on the POSS–2 optical frame. The source is resolved into a triple. The three components are labelled as A, B and C. The whole radio source is located within the optical galaxy and has a largest linear size of $\sim$35 kpc along the North-South axis. The axis of the central component A is misaligned with respect to the whole source elongation.

No other images at 1.4 GHz are available in the literature for this source, except for the NVSS and FIRST surveys. The total flux density of the source is given in Table 3, and is in good agreement with the 1.4 GHz NVSS value (Table 1), despite the different angular resolution. The amount of total flux density measurements for this source allowed us to study its integrated spectrum. Our analysis is reported in Sect. 5.2.

4.2. Clusters observed at 235 and 610 MHz

In this section we present the radio images of the clusters observed both at 235 MHz and 610 MHz (Table 2). For all sources the radio information at each frequency is summarised in Table 4, where we give the flux density, the 235 MHz–610 MHz spectral index, and the largest linear size as estimated from the 235 MHz image (unless specified otherwise). Individual information is listed for those sources whose structure can be unambiguously separated into more than one component. A brief morphological description of the sources is given below.

A 1775 – The rich Abell cluster A 1775 is known to host a binary galaxy system (dumb-bell galaxy) at its centre, with two optical components of similar luminosity, separated by a projected distance of 32 kpc (Parma et al. 1991). In Fig. 7 we show the GMRT full resolution radio images at 610 MHz (left panel) and 235 MHz (right panel) of A 1775. At 610 MHz (left panel, superposed on the optical image), we can clearly recognise the different radio structures associated with the two galaxies: the North-Western galaxy hosts a $\sim 30''$ ($\sim$42 kpc) double radio source, labelled D; a head-tail radio source, labelled HT and extending on a scale of $\sim 270''$ ($\sim$380 kpc), is associated with the companion galaxy. As clear from the 610 MHz image shown in left panel of Fig. 7, the radio tail has a multiply curved structure. The morphology of the dumb-bell system is consistent with the 1.4 GHz VLA image presented in Owen & Ledlow (1997).

In Table 4 we give the flux density at 235 MHz and 610 MHz and the spectral index for the whole system (D+HT) as well as for the individual radio galaxies.

For this source we carried out a spectral study, reported in 5.3.

A 2162 – The GMRT full resolution images at 235 MHz and 610 MHz of the source are shown in the right and left panels of Fig. 8 respectively. The source is characterised by two opposite lobes, with lack of a central compact component at both frequencies. The radio emission is weak and the surface brightness low. A similar double morphology without a central component was found also at 1.4 GHz by Owen & Ledlow (1997). The source has a linear size of $\sim 90 \times 38$ kpc. The total flux density of the source at 610 MHz and 235 MHz, and the spectral index value between these two frequencies are given in Table 4. We point out that the 235 MHz measurement is most likely underestimated, due to problems with the flux density scale of the secondary calibrator (see also note to Table 4), therefore the reported value for the spectral index should be taken with care. A detailed spectral study for this source is reported in Sect. 5.4.

A 2372 – The cD galaxy in A 2372 hosts a spectacular large radio source with a wide-angle-tail (WAT) morphology. Our GMRT full resolution images at 610 MHz and 235 MHz are shown in the upper and lower panels of Fig. 9 respectively. The total angular extent of the WAT (end to end) is $\sim 730''$, corresponding to a linear size of $\sim$850 kpc. Our images are in very good agreement with the morphologies observed with the VLA

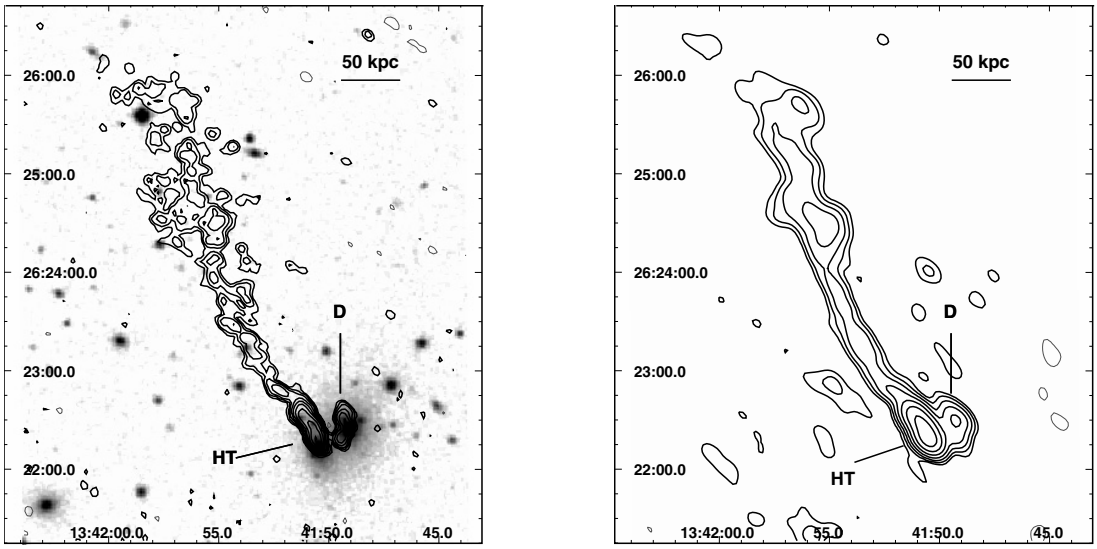

Fig. 7. A 1775 – GMRT radio contours at 610 MHz (*left panel*), overlaid on the POSS–2 optical frame, and 235 MHz (*right panel*) of the central cluster region. The 1σ level in the image is 130 μJy b^{-1} and 1.5 mJy b^{-1} respectively. Logarithmic contours are reported, starting from $\pm 3\sigma$. The contour peak flux is 118.3 mJy b^{-1} and 480.8 mJy b^{-1} in left and right panels respectively. The *HPWB* is 5.4″ × 4.2″, PA 49° in the 610 MHz image and 12.7″ × 9.1″, PA 63° in the 235 MHz image. D indicates the double radio source associated with the central cD galaxy, while HT stands for the head-tail radio galaxy associated with the companion galaxy. For this system 1″ = 1.41 kpc.

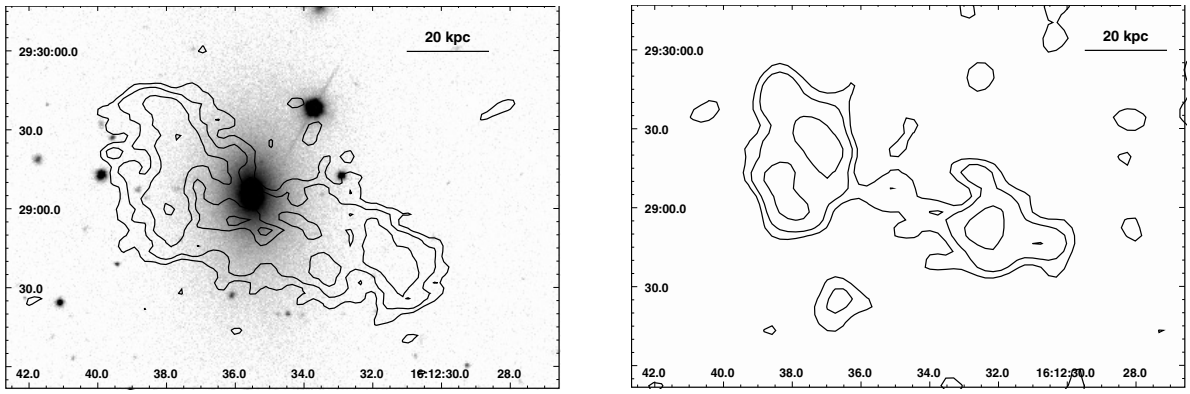

Fig. 8. A 2162 – GMRT radio contours at 610 MHz, overlaid on the SDSS optical frame (*left panel*), and 235 MHz (*right panel*) of the central radio galaxy. The 1σ level in the image is 150 μJy b^{-1} at 610 MHz and 1 mJy b^{-1} at 235 MHz. Logarithmic contours are reported, starting from $\pm 3\sigma$. The *HPWB* is 7.1″ × 4.9″, PA −83° in the left panel and 14.7″ × 10.8″, PA −85° in the right panel. For this source 1″ = 0.64 kpc.

at 1.4 GHz and 4.9 GHz and reported in Owen & Ledlow (1997) and Gregorini et al. (1994) respectively.

The central component, coincident with the optical cD galaxy (labelled as A in Fig. 9), shows a double morphology, as is clear from the insert in the upper panel of the figure, which zooms into the nuclear emission at 610 MHz. Such features are most likely the inner jets. On a larger scale, the jets show symmetric "wiggles" until they lose collimation and form the lobes (B and C in Fig. 9). A sharp edge in the western lobe suggests strong interaction with the intracluster medium, but unfortunatley no high resolution X-ray observations are available for this cluster to investigate the origin of this feature.

The total flux densities at 610 MHz and 235 MHz and the spectral index between these two frequencies are given in Table 4. A detailed spectral study is reported in Sect. 5.5.

A 2622 – Figure 10 presents the GMRT full resolution images of the source at 610 MHz (left panel) and 235 MHz (right panel). The whole source extends over a total size of ∼120 kpc. North and South of the bright central component A, two diffuse radio lobes are detected, labelled respectively as B and C in the left panel of the figure. Comparison of the images suggests that very low frequency emission is present in this source. A 2622 was observed with the VLA at 1.4 GHz at high resolution (A and B array) by Owen & Ledlow (1997). They could detect only component A in our images. At 4.7 GHz Ball et al. (1993) did not detect any radio emission from this galaxy at a sensitivity limit of 0.69 mJy.

The total flux density of the source at 235 MHz and 610 MHz and the resulting spectral index are given in Table 4, where we also give the 610 MHz flux density of the individual source components.

A detailed spectral analysis for this source is given in Sect. 5.6.

MKW 02 – The GMRT full resolution images at 235 MHz and 610 MHz are presented in Fig. 11. The central cD galaxy is associated with a very large radio galaxy (∼15′, ∼670 kpc), whose radio power is typical of FR I radio galaxies (see Table 1), but whose radio morphology is similar to that of FR II radio sources, with two jets, asymmetric in size and brightness, lobes and possibly hot spots.

At the resolution and frequency of our images only the central component associated with the cD galaxy (labelled as C in

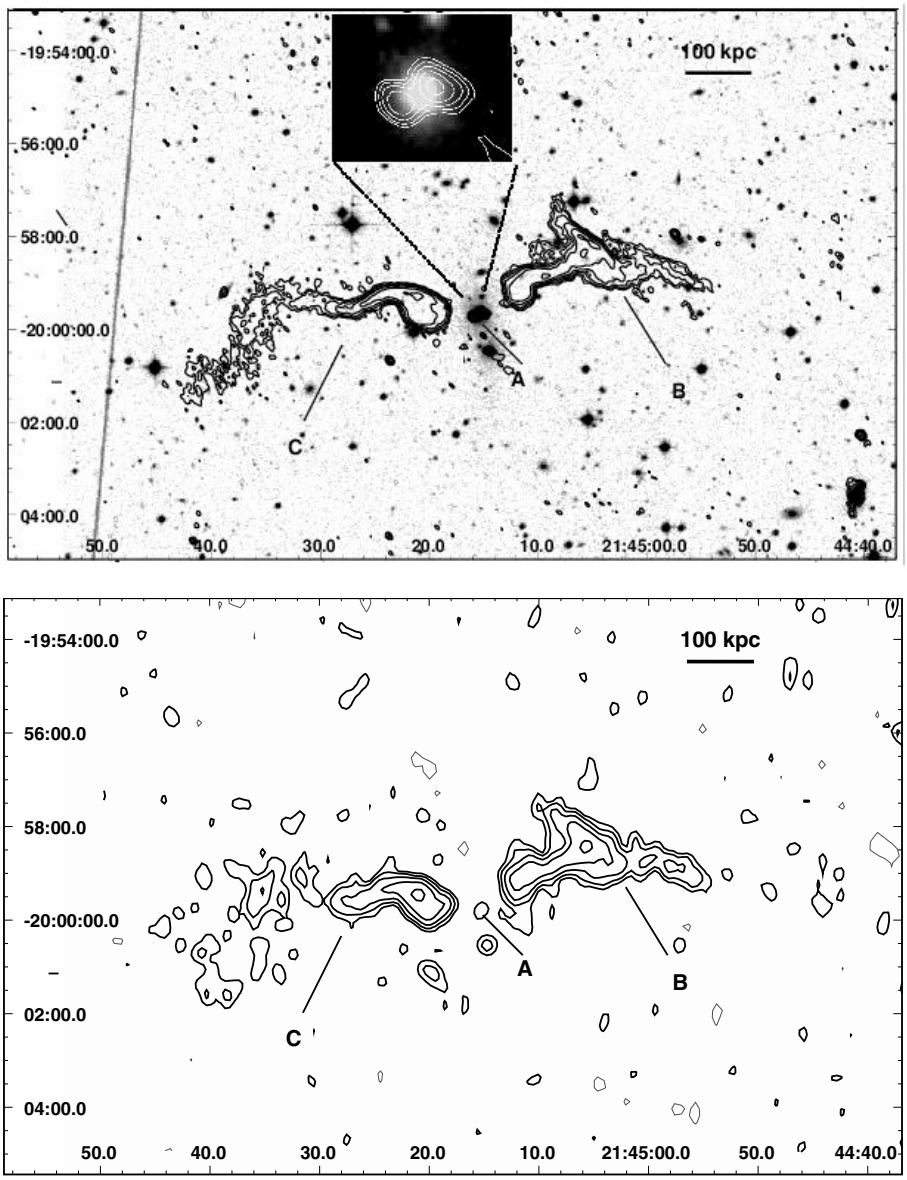

Fig. 9. A 2372 – GMRT 610 MHz, on POSS–2 optical image, (*upper panel*) and 235 MHz (*lower panel*) radio contours of the central radio galaxy overlaid on the POSS–2 optical frame. The 1σ level in the image is 65 μJy b^{-1} and 1.5 mJy b^{-1} respectively. In both panels logarithmic contours are reported, starting from $\pm 3\sigma$. The *HPWB* is $7.5'' \times 5.7''$, PA 38° in the 610 MHz image and $19.7'' \times 13.8''$, PA −8° at 235 MHz. In both panels letters A, B, and C indicate the different source components. For this source $1'' = 1.17$ kpc.

Fig. 11) and the outer regions of the lobes (labelled as A and B) are visible. The southern jet is completely resolved out at both frequencies, and hints of the northern one (D in Fig. 11) are visible only at 235 MHz. Our images are fully consistent with a 1.4 GHz VLA image reported in Burns et al. (1987).

The total flux density of the source at 235 MHz and 610 MHz and the derived spectral index are given in Table 4, where we also report the 610 MHz flux density and size of the source components.

The total flux density value at 610 MHz is most likely underestimated, even though no apparent calibration problem was encountered during the data reduction. We measured $S_{610\ \mathrm{MHz}} = 245$ mJy, to be compared with the value from the NVSS, i.e. $S_{1.4\ \mathrm{GHz}} = 385$ mJy. The 1.4 GHz flux density measured by Burns et al. (1987) is different from the NVSS one, being $S_{1.4\ \mathrm{GHz}} = 668$ mJy (resolution ∼13″). These values seem to disagree even if we allow for some variability of the central component, since it contains only a small fraction of the total flux (12% at 610 MHz). Such disagreements suggest that the u–v coverage is critical for a source large and complicated as this one. For this reason we think that the spectral index values reported in Table 4 should be taken with caution, and considered as upper limits to the value of α. Due to the uncertain values of the flux density we did not undertake any study of the radio spectrum.

4.3. Clusters observed at 235 MHz, 610 MHz and 1.28 GHz

In this section we present the radio images of the poor clusters MKW 07 and MKW 03s, observed with the GMRT at 235 MHz, 610 MHz and 1.28 GHz (Table 2). For these sources the radio information at each frequency is summarised in Table 5, where we give the flux density, the 235 MHz−1.28 GHz spectral index, and the largest linear size LLS, estimated from

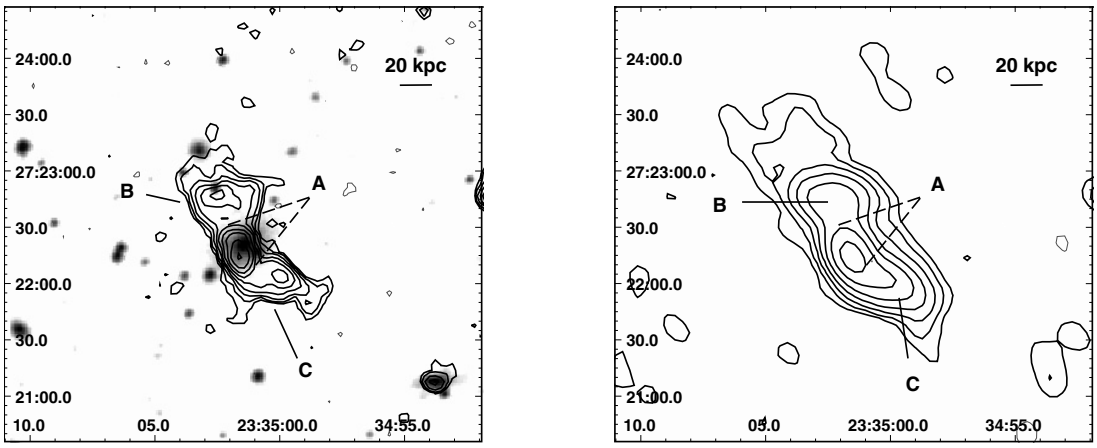

Fig. 10. A 2622 – GMRT radio contours at 610 MHz, overlaid on the POSS–2 optical image (*left panel*), and 235 MHz (*right panel*) of the central radio galaxy. The 1σ level in the image is 50 μJy b^{-1} and 800 μJy b^{-1} respectively. Logarithmic contours are reported starting from $\pm3\sigma$ and $\pm4\sigma$ in the left and right panel respectively. The *HPWB* is $4.9'' \times 4.2''$, PA 52° in the 610 MHz image and $17.1'' \times 11.4''$, PA 53° in the 235 MHz image. In the left panel the letters A, B, and C indicate the different source components. For this source $1'' = 1.18$ kpc.

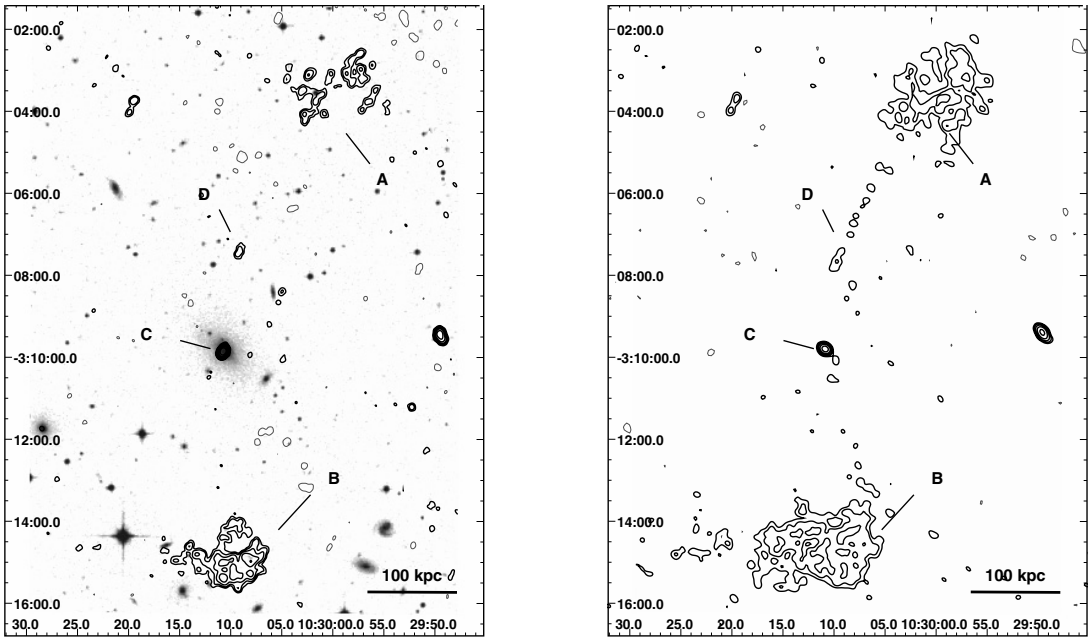

Fig. 11. MKW 02 – GMRT radio contours at 610 MHz, overlaid on the POSS–2 optical image (*left panel*), and 235 MHz (*right panel*) of the central radio galaxy. The 1σ level in the image is 130 μJy b^{-1} and 650 μJy b^{-1} respectively. Logarithmic contours are reported, starting from $\pm3\sigma$. The *HPWB* is $9.7'' \times 8.6''$, PA $-24°$ in the 610 MHz image and $12.1'' \times 9.7''$, PA 65° in the 235 MHz image. In both panels letters A, B, C, and D indicate the different source components. For this source $1'' = 0.75$ kpc.

the 235 MHz image (unless specified otherwise). The radio information is also given for each source component. Individual comments are reported below.

MKW 07 – The cD galaxy at the centre of the poor cluster MKW 07 is embedded in an asymmetric envelope, also including a compact fainter companion (Van den Bergh 1977). The radio emission from this galaxy is given in Fig. 12, where we present the full resolution images at 1.28 GHz, overlaid on the optical frame (left panel), 610 MHz (central panel) and 235 MHz (right panel). Note that the bright object west of the central cD galaxy is a star. At all frequencies the morphology of the source is dominated by two radio lobes, labelled A and B in the figure. The source has a largest linear size of ∼98 kpc in the 235 MHz image.

A compact component, labelled C and centered on the nucleus of the brightest galaxy, is clearly detected at 1.28 GHz (left panel of Fig. 12) and is visible also at the other two frequencies. No jets or other features connect the nuclear component C with the two lobes. On the other hand, the two lobes are connected by a bridge of emission, visible at 1.28 GHz and 610 MHz. This feature is reminiscent of the radio galaxy 3C 338, associated with the multiple nucleus galaxy at the centre of A 2199, whose morphology is interpreted as being an old radio galaxy with restarted nuclear activity (Giovannini et al. 1998).

The total flux density at each frequency and the spectral index between 235 MHz and 1.28 GHz are given in Table 5. The GMRT 1.28 GHz flux density measurement is in good agreement with the 1.4 GHz NVSS value (Table 1), despite the different angular resolution.

The total spectrum and a spectral index image for this source are discussed in Sect. 5.7.

Table 5. Radio source data at 235 MHz, 610 MHz and 1.28 GHz.

Cluster	component	$S_{235\ \mathrm{MHz}}$ (mJy)	$S_{610\ \mathrm{MHz}}$ (mJy)	$S_{1.28\ \mathrm{GHz}}$ (mJy)	$\alpha_{235\ \mathrm{MHz}}^{1.28\ \mathrm{GHz}} \pm 0.04$	LLS kpc
MKW 07	tot.	700	244	95	1.18	$\sim 98 \times 43$
	A	294	110	44	1.13	$\sim 43 \times 24$
	B	392	131	50	1.22	$\sim 43 \times 37$
	C	14	3	1	1.67	$\sim 1.6 \times 0.4^{\diamond}$
MKW 03s	tot.	8436	1010	139	2.42	$\sim 170 \times 80$
	A	7810	952	119	2.47	$\sim 98 \times 90$
	B	586	40	10	2.40	$\sim 58 \times 53$
	C	40	18	10	0.82	<9

$^{\diamond}$ This value is estimated from the 1.28 GHz image.

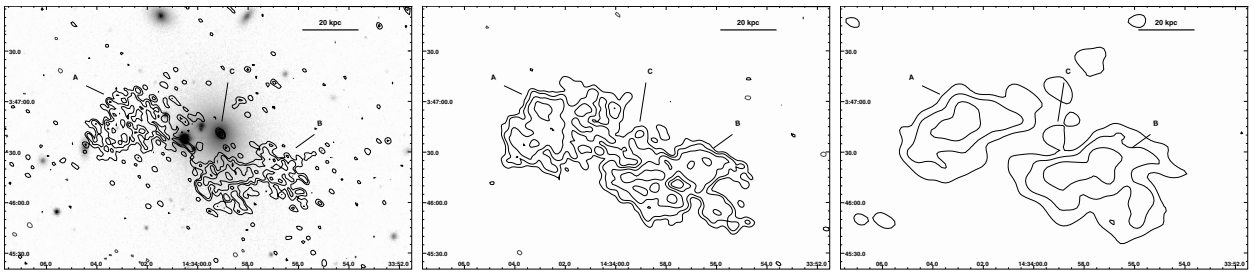

Fig. 12. MKW 07 – GMRT radio contours at 1.28 GHz, overlaid on the SDSS optical frame (*left panel*), 610 MHz (*central panel*) and 235 MHz (*right panel*) of the central radio galaxy. The 1σ level in the image is 30 μJy b^{-1}, 100 μJy b^{-1} and 1.5 mJy b^{-1} respectively. Logarithmic contours are reported, starting from $\pm 3\sigma$. The contour peak flux is 0.96 mJy b^{-1} in the left panel, 3.52 mJy b^{-1} in the central panel, and 33.51 mJy b^{-1} in the right panel. The *HPWB* is 3.5″ × 2.4″, PA 49° at 1.28 GHz, 5.8″ × 4.4″, PA 57° at 610 MHz and 14.0″ × 9.1″, PA 50° at 235 MHz. In all panels letters A, B and C indicate the different components of the source. For this source 1″ = 0.61 kpc.

MKW 03s – In Fig. 13 we present the new GMRT 235 MHz image of the source and refer to Mazzotta et al. (2004) and Giacintucci et al. (2006) for the GMRT radio images at 1.28 GHz and 610 MHz. As observed at 1.28 GHz, 610 MHz, and at 327 MHz (VLA data, de Young 2004, also reported in Mazzotta et al. 2004), the source shows two opposite radio lobes. The southern one (labelled as A) is brighter than the northern one (labelled as B). A compact component (labelled as C) is detected coinciding with the nucleus of the cD galaxy. The flux density of the various source components at 235 MHz are reported in Table 5, where we summarise the values at 610 MHz and 1.28 GHz, taken from Mazzotta et al. (2004). The radio emission from the cD in MKW 03s is dominated at all the frequencies by the southern lobe A, which accounts for most of the total flux density of the source. A study of the total spectrum of this source is reported in Sect. 5.8.

A combined radio (GMRT 1.28 GHz and 610 MHz) and X-ray analysis of the cD radio source in MKW 03s has been published in Mazzotta et al. (2004) and Giacintucci et al. (2006). In those papers we discussed the connection between the radio activity of the central AGN and the features observed in the X-ray surface brightness and temperature structure of the cluster. MKW 03s shows two opposite cavities in the X-ray surface brightness, filled by the radio emission from the lobes of the central radio galaxy. The lobes appear confined by extended gas regions with temperatures significantly higher than the radially averaged gas temperature at any radius. A possibile interpretation of this complex X-ray structure is that the radio lobes are expanding into the external ICM and heating the gas. Hence, MKW 03s may be an example of gas heated by the central AGN. A preliminary analysis of the synchrotron spectrum of the lobes provides radiative ages in reasonable agreement with this scenario (Mazzotta et al. 2004). A study of the implications of the possible connection between the morphological and spectral properties of the source and the cluster thermal structure will be discussed in detail in a forthcoming paper.

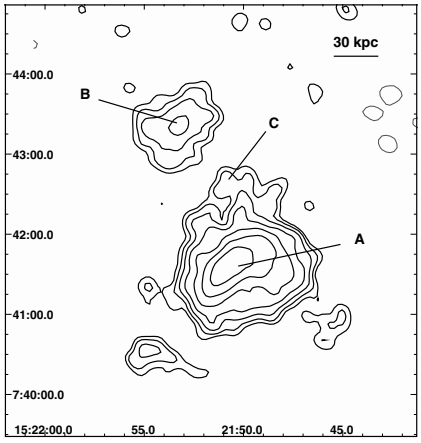

Fig. 13. MKW 03s – GMRT 235 MHz radio contours of the central radio galaxy., The 1σ level in the image is 2 mJy b^{-1}. Logarithmic contours are reported, starting from ± 6 mJy b^{-1}. The *HPWB* is 12.1″ × 9.1″, PA 52°. Letters A, B and C the different source component. For this source 1″ = 0.89 kpc.

4.4. Linear sizes and the cluster environment

The study of radio galaxies located at the cluster centres raises the question of whether the external dense intracluster medium confines the radio structure, affecting their morphology and limiting their total size.

Ledlow et al. (2002) compared the size distribution of radio galaxies as a function of the radio power for cluster and non–cluster sources (including both FR I and FR II types), and

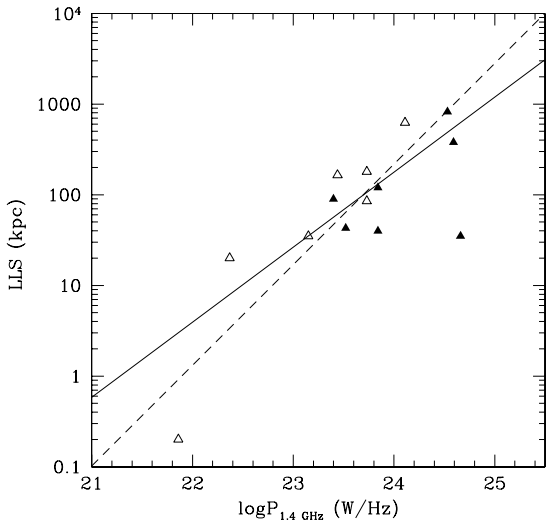

Fig. 14. 1.4 GHz radio power-radio size diagram for the combined rich (filled triangles) and poor (empty triangles) cD cluster sample.

found no significant difference between the two samples. Using the combined cluster-non cluster sample, they found that the linear size of FR I sources tends to increase with increasing radio power, while they did not find any dependence between radio power and size for FR II sources.

Radio galaxies at the cluster centres represent the extreme population of cluster radio galaxies. Using the radio power in Table 1 and the size from our 1.28 GHz (or 610 MHz) images (see Tables 3−5) we plotted the $\log P$ – LLS diagram for the cD galaxies under discussion here, as reported in Fig. 14. The sources located at the centre of the rich Abell clusters are indicated as filled triangles, while empty triangles represent the sources in poor clusters. Our sample covers only a part of the wide radio power range explored by Ledlow et al. (2002), since our objects have radio powers from $P_{1.4\ \mathrm{GHz}} \sim 10^{22}$ W Hz^{-1} to $P_{1.4\ \mathrm{GHz}} < 10^{25}$ W Hz^{-1}. Within this interval of radio power, the linear size distribution of our sources mainly extends over two orders of magnitude, being contained in the LLS range 10−1000 kpc (Fig. 14). The only exception is the unresolved radio galaxy in MKW 01s (Sect. 4.1), which is the least powerful source in our sample and has a size upper limit of only 0.2 kpc. We note that the observed range of source size is consistent with what expected in this radio power range from the ($P_{1.4\ \mathrm{GHz}}$, LLS) diagram in Ledlow et al. (2002). The fit obtained using the whole sample is LLS $\propto P_{1.4\ \mathrm{GHz}}^{1.11\pm0.19}$ (solid line in Fig. 14), while, excluding the MKW 01s data point, we find LLS $\propto P_{1.4\ \mathrm{GHz}}^{0.83\pm0.13}$ (dashed line).

The fit obtained using only the Abell clusters, LLS $\propto P_{1.4\ \mathrm{GHz}}^{1.01\pm0.19}$, is consistent within the errors with the fit obtained using only the poor clusters, i.e. LLS $\propto P_{1.4\ \mathrm{GHz}}^{1.36\pm0.21}$ (LLS $\propto P_{1.4\ \mathrm{GHz}}^{0.86\pm0.16}$ if we exclude MKW 01s). This consistency, however, may be affected by the large errors in the fit, due to the limited statistics of our sample. A similar analysis on a larger sample may allow us to draw a firmer conclusion on this issue.

We note that the most powerful radio sources are located in rich clusters, while the least powerful is located in a poor group.

5. Spectral analysis

For a number of sources, the information presented in this paper, coupled with literature and archival data, allowed us to carry out a radio spectral study to address the questions of the source radiative age and the kinematics. In this section we perform two types of analysis: *(a)* fit of the integrated radio spectrum, and *(b)* fit of the trend of the two-point spectral index along the source structure.

(a) For eight sources we obtained integrated source spectra making use of the database CATS (Verkhodanov et al. 1997), and fitted them with the Synage++ package (Murgia 2001). A continuous injection model (CI, i.e. the source is fuelled at a constant rate, Kardashev 1962) was adopted for the spectral fitting. The derived injection spectral index α_{inj} and the break frequency ν_{b} were then used to estimate the equipartition magnetic field B_{eq}, and the the radiative age t_{rad} of the source, using the following equation:

$$t_{\mathrm{rad}} = 1590 \frac{B_{\mathrm{eq}}^{0.5}}{(B_{\mathrm{eq}}^2 + B_{\mathrm{CMB}}^2)} [(1+z)\nu_{\mathrm{b}}]^{-0.5} \quad (1)$$

where t_{rad} is expressed in Myr, ν_{b} in GHz, B_{eq} and B_{CMB} in μG, with $B_{\mathrm{CMB}} = 3.2(1+z)^2$ is the magnetic field strength with energy density equal to that of the cosmic microwave background (CMB) at the redshift z.
For the ultra steep spectrum source in MKW 03s, a diffusion MJP model (Slee et al. 2001) provided the best fit to the total spectrum (see Sect. 5.8 for details). The model accounts for the diffusion of the synchrotron electrons in a magnetic field with a Gaussian distribution of field strengths (Murgia, in prep.). In this case the radiative lifetime of the electrons was calculated according to the equation

$$t_{\mathrm{rad}} = 1590 \frac{B_{\mathrm{rms}}^{0.5}}{(B_{\mathrm{rms}}^2 + B_{\mathrm{CMB}}^2)} [(1+z)\nu_{\mathrm{b}}]^{-0.5} \quad (2)$$

where B_{rms} is the mean field value over the distribution of field strengths.

(b) For five sources we performed a point-to-point spectral analysis carried out on two sets of images produced using the same $u-v$ range and cellsize, and restored with the same beam. The individual images were corrected for the primary beam attenuation, aligned and clipped at the 3σ level, and finally combined to obtain the spectral index map. For each source, details on the images and frequencies used for the analysis are given below in the appropriate sections. In each case we determined the average spectral index in circular regions, starting from the inner edge of each lobe and going outwards along the major axis, and derived the spectral index distribution as a function of distance from the core. The size of the regions selected for our analysis was chosen large enough to ensure a sufficient signal-to-noise-ratio and independent data points.
We fitted the trend following Parma et al. (1999 and 2002). In particular, we used the relation $\nu_{\mathrm{b}} \propto x^{-2}$, x being the distance from the core. Such a relation is expected if a constant expansion velocity is assumed (i.e. $x \propto t$), and reflects the fact that the radiating electrons become older as they move away from the nucleus, which is appropriate for the type of sources discussed here (FR I radio galaxies).
As detailed in the individual sections, the five sources studied here differ in their properties, and different models were used to obtain the best fit.

For all sources, B_{eq} was computed assuming a cut-off in the minimum energy for the radiating electrons corresponding to a Lorentz factor $\gamma = 50$ (Brunetti et al. 1997). The equipartition

Table 6. Equipartition fields and radiative ages from the analysis of the radio spectrum.

Source	α_{obs}	α_{inj}	ν_b GHz	B_{eq} 10^{-6} G	t_{rad} Myr	v_{growth} (c)
A 2480	0.6	0.55	8.4	∼10	15	0.8×10^{-3}
AWM 05	0.8	0.58	1.1	∼7	65	0.2×10^{-3}
A 1775	1.0	0.6	0.6	∼8	490	0.3×10^{-2}
A 2162	1.0	0.73	1.4	∼3	110	0.3×10^{-2}
A 2372	1.3	0.65	0.7	∼2	150	0.3×10^{-1}
A 2622	1.7	0.7*	0.5	∼4	150	0.5×10^{-2}
MKW 03s	1.9	0.7*	0.03	♣	21	0.8×10^{-1}

* Fixed in the fit.
♣ see Sect. 5.8.

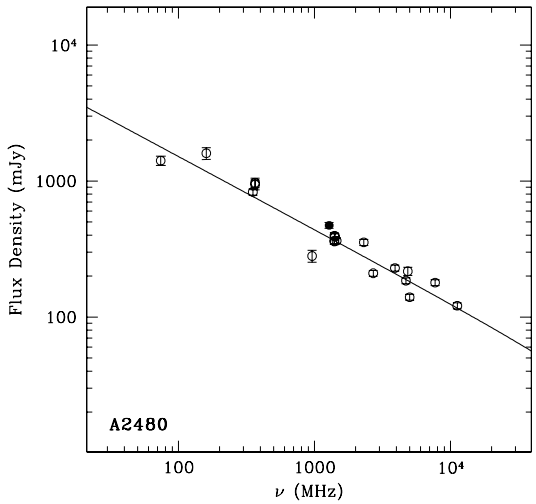

Fig. 15. A 2480 – Radio spectrum of the central radio galaxy between 74 MHz and 11.2 GHz. The empy circles are literature data, the filled circle is the GMRT 1.28 GHz value. The solid line is the best fit of the CI model.

magnetic field was derived using the injection index of the radiative electrons, scaling the radio flux density to the value expected for α_{inj}.

Our analysis is presented in detail in the following subsections for each source individually, and the results are summarised in Table 6, where we list the observed spectral index α_{obs}, the injection spectral index α_{inj}, the frequency break ν_b, the equipartition magnetic field B_{eq}, the radiative age t_{rad} and a crude estimate of the source velocity growth v_{growth}/c, obtained assuming a constant velocity and using the linear sizes reported for each source in Tables 3−5, i.e. $v_{growth} = LLS/t_{rad}$.

Where possible, we report the values derived from the point-to-point analysis, in all other cases the results from the fit of the integrated spectrum are given.

5.1. A 2480. Integrated spectrum and spectral trend along the jets

We used our 1.28 GHz flux density in Table 3, the flux densities reported in the literature and the 74 MHz VLSS measurement to derive the total synchrotron spectrum of the source, shown in Fig. 15. The spectrum can be described as a power law with $\alpha = 0.6$ in the 160 MHz−11.2 GHz frequency range. Below 160 MHz the spectrum has a negative slope with $\alpha = -0.2$.

As clear from Fig. 15, the integrated spectrum is scattered, however it is still consistent with a single power law. The fit, shown as a solid line in the figure, gives $\alpha_{inj} = 0.54 \pm 0.03$.

In Fig. 16 (left panel) we show the spectral index image of the source (colours), obtained by comparison of the GMRT 1.28 GHz image and the 4.87 GHz image (contours) from VLA archival data which we re-analyzed (Obs. Id. AB398). The figure shows the presence of a central flat spectrum region with $\alpha = 0.2 \pm 0.1$. Both jets and lobes in the source have an average spectral index $\alpha \sim 0.7 \pm 0.1$. These features suggest that the radio source is currently fed by an active nucleus.

Using the spectral index image, we derived the average spectral index of the source along the two jets. The distribution of α is given in the right panel of Fig. 16, and the insert shows the circular regions used during the analysis (red open circles overlaid on the contour image). The spectrum steepens along the jet from ∼0.6 at the jet basis to ∼1 in the outer regions. We interpreted the spectral trend along the lobes in terms of radiative ageing of the relativistic electrons by synchrotron and inverse Compton processes (e.g. Parma et al. 1999, and references therein). It is assumed that the radiative losses dominate over expansion losses and re-acceleration processes. The spectral trend was fitted with a simple JP model (Jaffe & Perola 1974). This model assumes an isotropic distribution of the pitch angles of the radiating electrons with respect to the local direction of the magnetic field. This condition is likely to be satisfied in most sources of our sample since the inverse Compton energy losses due to the microwave background radiation are as important as the synchrotron losses, and in the former random orientations are expected between electrons and photons. The JP model is characterized by three free parameters: i) the injection spectral index α_{inj}, ii) the break frequency ν_b, and iii) the flux normalization. By assuming a constant magnetic field across the source and a constant speed for the plasma outflow, we can obtain the injection spectral index and the minimum break frequency from a global fit of the observed spectral index profiles. The model fit, which is represented by the blue lines in Fig. 16, provided $\alpha_{inj} = 0.55 \pm 0.03$, $\nu_b = 8.4^{+2.5}_{-1.6}$ GHz, the magnetic field obtained with this analysis is again $B_{eq} = 10$ μG and the derived radiative age is $t_{rad} = 1.5 \times 10^7$ yr. Part of the observed spectral steepening could be due to a decrease of the magnetic field strength with the increasing distance from the core. If this is the case, the radiative age reported above should be considered as an upper limit to the source age.

5.2. AWM 05. Study of the integrated spectrum

Beyond the flux density data reported here (1.28 GHz, GMRT, Table 3 and 1.4 GHz, NVSS, Table 1), 74 MHz and 2.38 GHz flux density measurements are also available in the literature (VLSS and Dressel & Condon 1978 respectively). The resulting integrated spectrum is reported in Fig. 17, and the spectral index in the range 74 MHz−2.38 GHz is $\alpha = 0.8$.

We assume that the integrated radio source spectrum is described by a continuous injection model (CI), where the source is continuously replenished by a constant flow of fresh relativistic particles with a power law energy distribution. Under these assumptions, it is well known that the radio spectrum has a standard shape (Kardashev 1962), with spectral index α_{inj} below a critical frequency ν_b and $\alpha_h = \alpha_{inj} + 0.5$ above ν_b. The CI spectral fit allows us to determine the non-aged spectral index α_{inj} and the break frequency ν_b, which are the free parameters characterizing the model together with the flux normalization. The CI model applies to those sources whose total spectrum is dominated by the emission from the lobes, which accumulated most

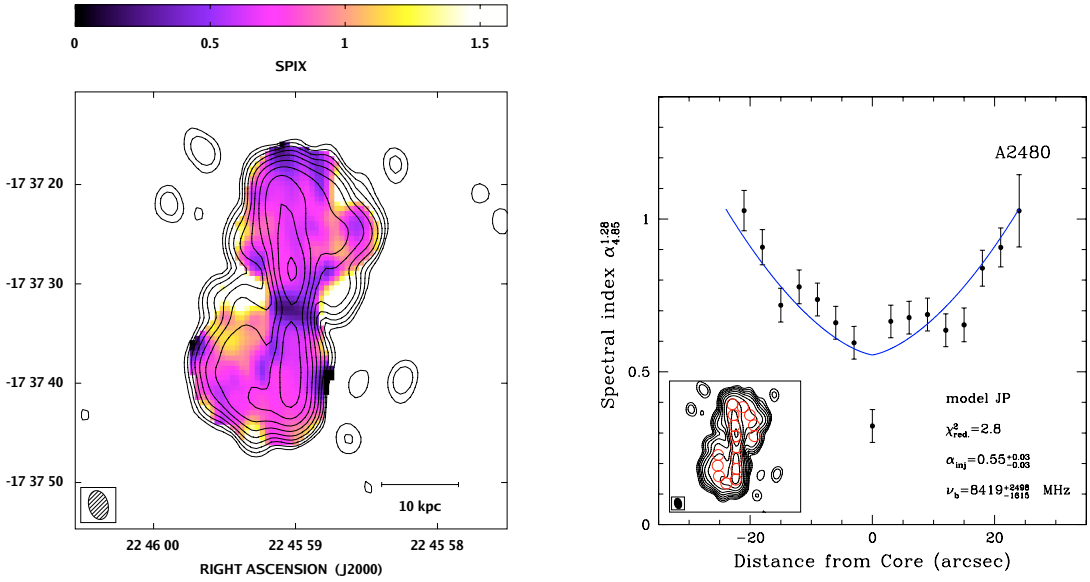

Fig. 16. A2480 – *Left*: colour scale image of the spectral index distribution between 1.28 GHz and 4.87 GHz over the central radio galaxy. It has been computed from images with a restoring beam of 2.9″ × 2.0″. Overlaid are the VLA 4.87 GHz contours at levels 0.15, 0.30, 0.60, 1.20, 2.40, 4.80, 9.60 and 19.20 mJy. *Right*: 1.28−4.87 GHz spectral index distribtion along the jets as function of distance from the core. The solid lines represent the best fit of the radiative model described in the text.

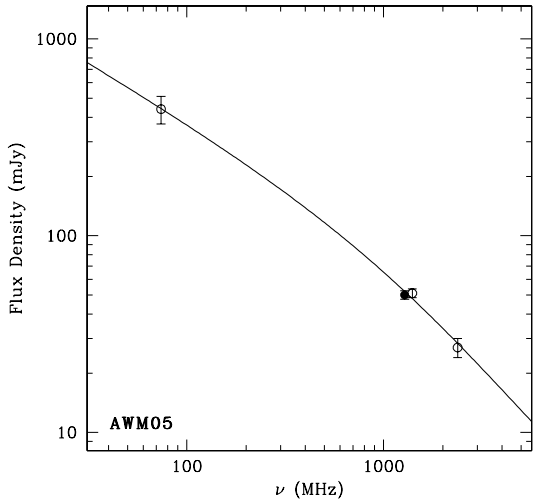

Fig. 17. AWM05 – Radio spectrum of the central radio galaxy between 74 MHz and 2.38 GHz. The empy circles are literature data (see text), the filled circle is the GMRT 1.28 GHz value. The solid line is the best fit of the CI model.

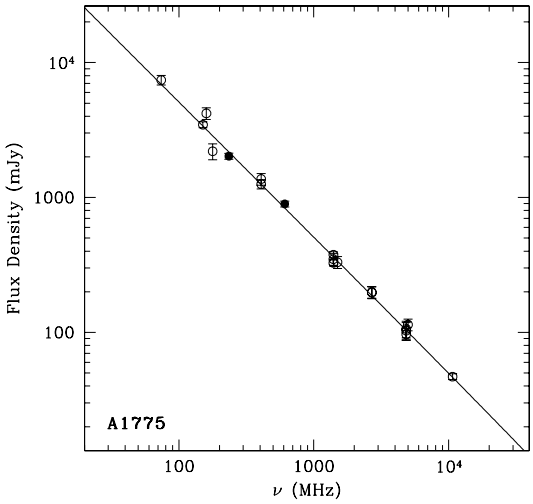

Fig. 18. A 1775 – Radio spectrum of the central source between 74 MHz and 10.7 GHz (the head tail and the double source are considered together), as derived from the GMRT 235 MHz and 610 MHz (filled circles) and literature data (empty circles). The solid line is the best fit of the CI model.

of the electrons produced over the entire source life. If the radiative losses are dominant over the expansion losses and the magnetic field is constant, the break frequency may be used to estimate the time elapsed since the source formation using Eq. (1).

The best fit of the CI model to the integrated spectrum of AWM 05 is reported in Fig. 17 (solid line), and provides a break frequency ν_b = 1.1 GHz, and $\alpha_{inj} = 0.58^{+0.25}_{-0.18}$. The equipartition magnetic field and radiative age for the relativistic electrons are respectively $B_{eq} \sim 7$ μG and $t_{rad} = 6.5 \times 10^7$ yr (see Sect. 6.3 and Table 6).

For this source the radio spectrum is poorly constrained, and the parameters obtained with the fit should be considered as indicative.

5.3. A 1775. Spectral analysis along the tail

We used the flux densities in Table 4 and the literature values (which include both the head-tail and the double source) to derive the integrated synchrotron spectrum of the whole radio emission associated with the dumb-bell system. The resulting spectrum is shown in Fig. 18. It can be fitted with a single power law with α = 1.0 between 74 MHz and 10.7 GHz. Figure 18 clearly shows the reliability of the GMRT flux density measurements at 610 MHz and 235 MHz presented here.

From the flux density values given in Table 4 it is clear that the long head-tail radio galaxy is the dominant component in the total spectrum. The 235 MHz−1.4 GHz radio spectra of the head-tail and the double separately are shown in Fig. 19, where we used the 1.4 GHz flux densities from the FIRST survey

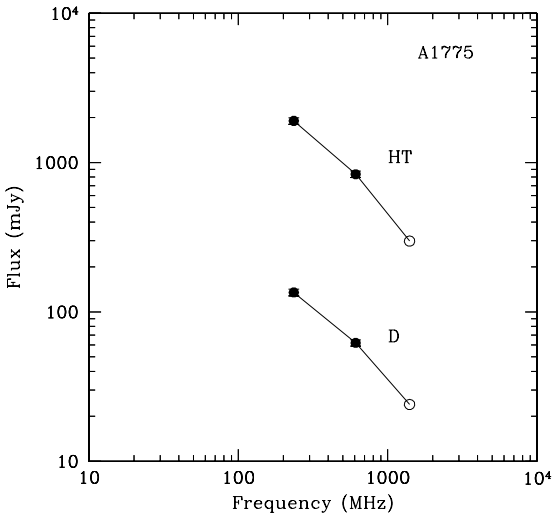

Fig. 19. A 1775 – Radio spectrum of the double (D) and head-tail (HT) radio galaxies. The 1.4 GHz flux density values for both sources are from the FIRST survey (empty circles). The filled circles are the GMRT 235 and 610 MHz data.

(Table 1). The two spectra are very similar, and can be described as a power law with spectral index $\alpha_{235}^{1400} \sim 1.0$.

In Fig. 20 (left panel) we show the spectral index image of the two sources. The image is obtained by comparison of the 235 MHz image (contours) and the 610 MHz image (not shown here). There is a clear separation in the spectral index distribution between the region dominated by the head of the tailed radio galaxy ($\alpha \sim 0.6-0.8$), and the double source, the latter being steeper, with an average value of $\alpha = 1.0 \pm 0.2$, consistent with the spectrum in Fig. 19. There is no obvious gradient in the spectral index along the tail of the head-tail source, which appears rather uniform with an average value of $\langle\alpha\rangle \sim 1.5 \pm 0.3$.

We carried out the spectral index analysis along the tail of A 1775, following the approach described above. The spectral index (right panel of Fig. 20) steepens from ∼0.8 to ∼1.2−1.4 within the first arcmin from the head, then it remains fairly constant.

In Sect. 5.1, we analyzed the spectral profiles in A2480 assuming that the dominant processes producing the energy losses of the relativistic electrons are synchrotron and inverse Compton, neglecting both adiabatic expansion and re-acceleration. With the additional assumption of a constant advance speed of the synchrotron plasma, we found that the fit of the JP model to the data well describes the overall trend of the observed spectral index as a function of the distance from the core. However, in A 1775 we observe a saturation of the spectral index along the tail. This suggests that the break frequency decreases only in the initial part of the tail, and remains constant going further out. A possible explanation of this behaviour is that re-acceleration processes are at work, which would partly compensate for the radiative energy losses and cause a freezing of the break energy at that value where the radiative and the acceleration time scales are equal. The spectral index trend in A 1775 was therefore fitted with a modified JP model.

In particular, a JP model was considered, under the assumption that the radio galaxy moves through the intergalactic medium at constant speed, and that the radiating electrons undergo radiative losses and are systematically reaccelerated on a Fermi timescale t_F (see Parma et al. 1999).

Under such an hypothesis, the break frequency scales with time, and hence with the distance along the tail, according to the following:

$$\nu_b \sim \frac{B_{eq}}{[(B_{eq}^2 + B_{CMB}^2 \times t_F \times (1 - e^{(-t_{rad}/t_F)})]^2}. \quad (3)$$

Note that for $t_{rad} \ll t_F$, the above equation provides the "classical" scaling

$$\nu_b \sim \frac{B_{eq}}{[(B_{eq}^2 + B_{CMB}^2) \times t_{rad}]^2} \quad (4)$$

while for $t_{rad} \gg t_F$ the break frequency is frozen to the value

$$\nu_b \sim \frac{B_{eq}}{[(B_{eq}^2 + B_{CMB}^2) \times t_F]^2}. \quad (5)$$

The reacceleration modifies the shape of the spectrum in the "oldest" part of the tail, where $t_{rad} > t_F$.

The fit provides a break frequency $\nu_b = 644^{+195}_{-120}$ MHz, and $\alpha_{inj} = 0.6 \pm 0.1$. These values yield an equipartition magnetic field $B_{eq} = 8\ \mu$G.

The reacceleration model provides a Fermi scale $t_F = 6.9^{+0.7}_{-0.8} \times 10^7$ yr, a radiative age $t_{rad} = 4.9 \pm 2.5 \times 10^8$ yr and a galaxy velocity $v_{gal} = 755^{+299}_{-249}$ km s^{-1}.

The fit of the simple JP model without re-acceleration (not shown) yields a radiative age of $t_{rad} \simeq 5.9 \times 10^7$ yr. This value would underestimate the source age by almost an order of magnitude and hence lead to an implausibly high advance speed for the galaxy through the ICM, i.e. $v_{gal} \simeq 6300$ km s^{-1}.

5.4. A 2162. Study of the integrated spectrum

In order to derive the total synchrotron spectrum of the source over a wide range of frequencies, we used the 610 MHz flux densities (Table 4), and the literature values. The spectrum is shown in Fig. 21, with the best fit superposed (solid line). The GMRT 235 MHz measurement is most likely understimated, due to problems with the flux density scale of the secondary calibrator (see Sect. 4.2). For this reason, this value was not used for the spectral fit. The derived integrated spectrum, shown in Fig. 21, has a power law shape with an average spectral index $\alpha = 1.0$ in the frequency range 151 MHz−4.7 GHz.

No strong jets, core or hot spots are present in this source and thus its total emission is likely to be dominated by the emission from the lobes. We therefore apply the CI model to the study of its integrated spectrum. The spectral fit of the CI model provided $\alpha_{inj} = 0.73^{+0.09}_{-0.08}$ and $\nu_b = 1.4^{+1.8}_{-0.72}$ GHz. With these values the estimated equipartition magnetic field and radiative age of the electrons are respectively $B_{eq} \sim 3\ \mu$G and $t_{rad} = 1.1 \times 10^8$ yr (see Sect. 6.3 and Table 6).

5.5. A 2372. Spectral analysis along the lobes

For this sources we apply both the CI model to the study of the integrated spectrum and the JP model to the study of the spectral profiles along the lobes.

We used our flux density measurements (Table 4), the flux density obtained on the 4.9 GHz image from VLA archival data (Obs. ID AG0293), and collected the literature data for this radio galaxy to derive the total radio spectrum in the range 74 MHz−4.9 GHz, which we report in Fig. 22. The GMRT flux density values nicely fit the gap between 74 MHz and 1.4 GHz.

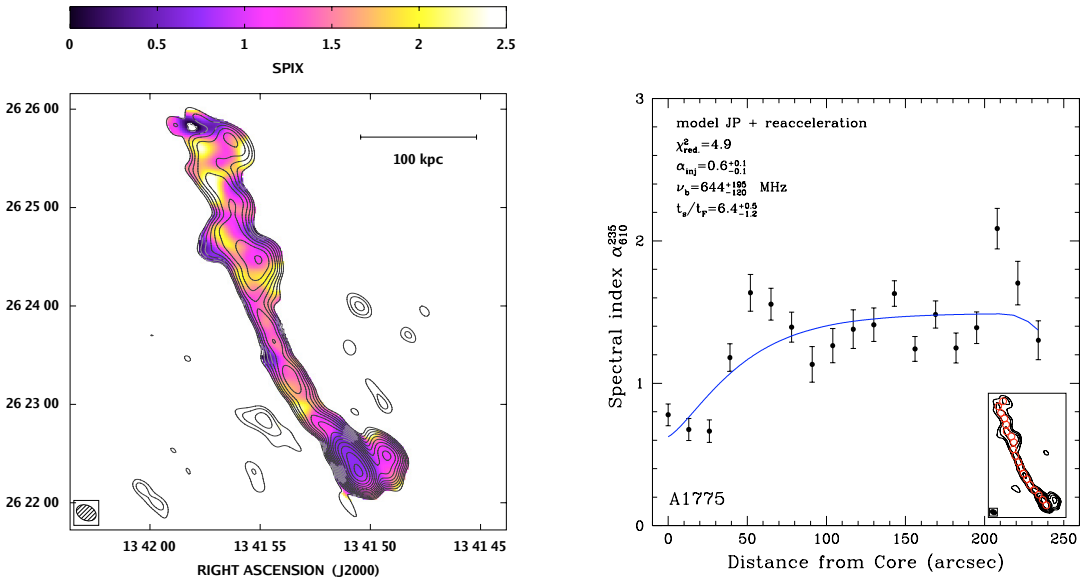

Fig. 20. A 1775 – *Left*: colour scale image of the spectral index distribution between 235 MHz and 610 MHz over the head-tail radio galaxy and the double source, as computed from images with a restoring beam of 12.7″ × 9.1″. Overlaid are the GMRT 235 MHz contours at levels 4.5, 9, 18, 36, 72, 144, 288 mJy. *Right*: distribution of the spectral index along the tail.

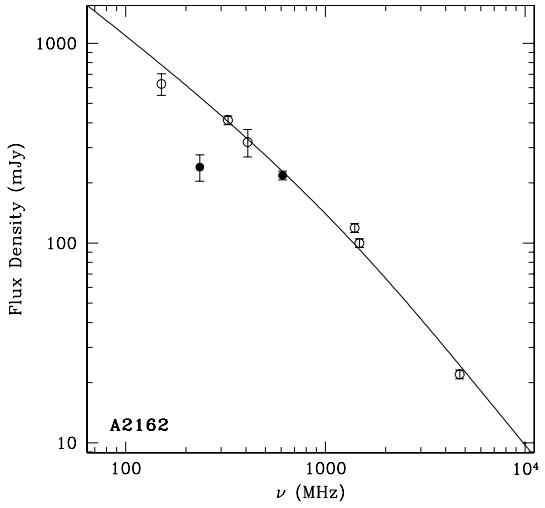

Fig. 21. A 2162 – 74 MHz–4.7 GHz radio spectrum of the central radio galaxy, as derived from literature data (empty circles) and the GMRT 235 MHz and 610 MHz values (filled circles). Note that the 235 MHz value is unreliable due to problems with the secondary calibrator. The solid line is the best fit of the CI model.

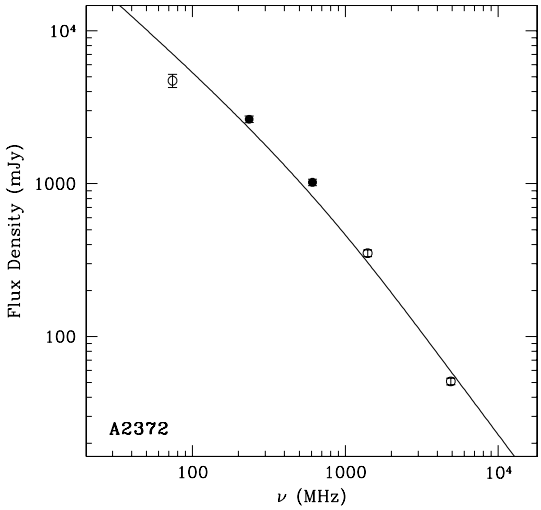

Fig. 22. A 2372 – Radio spectrum of the central radio galaxy between 74 MHz and 4.9 GHz. The empty circles are literature data, while the filled circles are the 235 MHz and 610 MHz measurements. The solid line is the best fit of the CI model.

The spectral index is $\alpha = 1.3$ in the 235 MHz–4.9 GHz frequency range, and it flattens below 235 MHz.

The best fit of the CI model to the spectrum is shown with a solid line in Fig. 22, and provides a break frequency $\nu_b = 0.94^{+0.70}_{-0.38}$ GHz and $\alpha_{inj} = 0.84^{+0.03}_{0.05}$. The estimated average magnetic field and radiative lifetime of the source are respectively $B_{eq} \sim 2\,\mu$G and $t_{rad} \sim 1.5 \times 10^8$ yr.

For this source it was possible to image the spectral index distribution in the range 235−610 MHz and to fit the spectrum of each lobe. The spectral index image and the spectral trend along the lobes are given in Fig. 23 (left and right respectively).

The synchrotron spectrum of the source between 235 MHz and 610 MHz is inverted in the core region ($\alpha \sim -0.5$), while the spectral index steepens from 0.7 ± 0.1 to 1.0 ± 0.1 along the jets. In the outer regions of the tails the spectrum further steepens, up to $\alpha = 2.0 \pm 0.3$.

We estimated the radiative ages of the radio lobes (B and C in Fig. 9) by fitting their spectral index distribution as function of the distance from the core with a simple JP model as performed for A2480 (see Sect. 5.1). The model fit provided $\alpha_{inj} = 0.56 \pm 0.04$ and $\nu_b = 680^{+260}_{-150}$ MHz, for both lobes. Using these values we estimated an average equipartition magnetic field $B_{eq} \sim 2\,\mu$G and a radiative lifetime $t_{rad} = 1.5 \pm 0.2 \times 10^8$ yr for both the lobes. These estimates are in very good agreement with the magnetic field and radiative age provided by the fit of the whole source spectrum (Table 6). The CI spectral shape should indeed represent the sum of a series of JP spectra with ages ranging from zero up to the age of the source, while the break frequency of the oldest JP spectrum present in the source should correspond to the break frequency of the CI model.

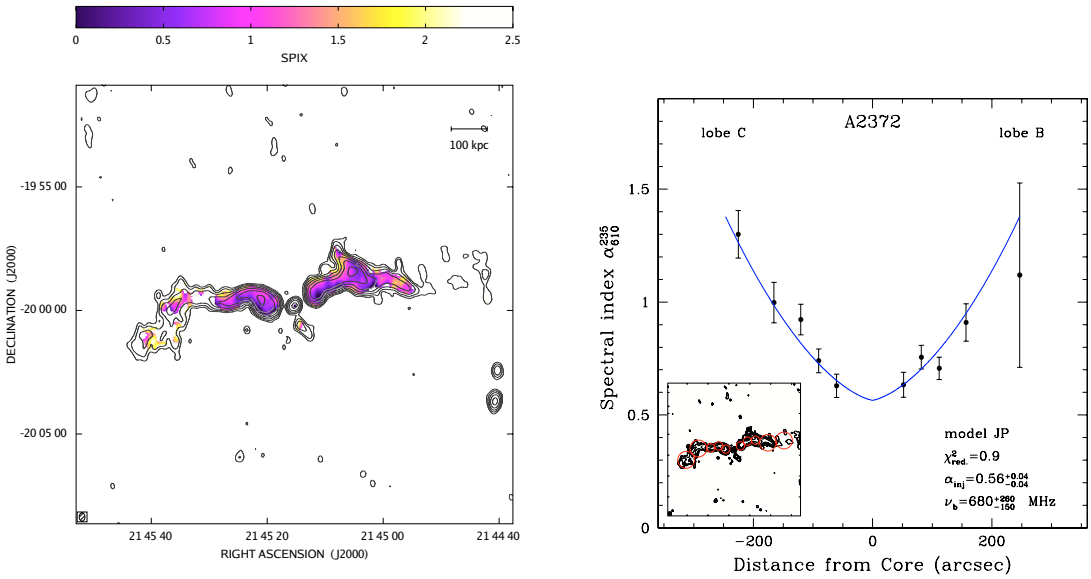

Fig. 23. A 2372 – *Left*: colour scale image of the spectral index distribution between 235 MHz and 610 MHz over the WAT radio galaxy at the cluster centre, derived using images with a restoring beam of 20.0″ × 14.0″. Overlaid are the GMRT 610 MHz contours at levels 0.6, 1.2, 2.4, 4.8, 9.6 mJy. The error in the spectral index at 1σ level ranges from ±0.05 and to ±0.1 along the jets, and is ±0.3 at the core and at the end of the tails. *Right*: 235 MHz−610 MHz spectral index distribution of the lobes as function of the distance from the core. The solid line are the best fit of the radiative model described in the text.

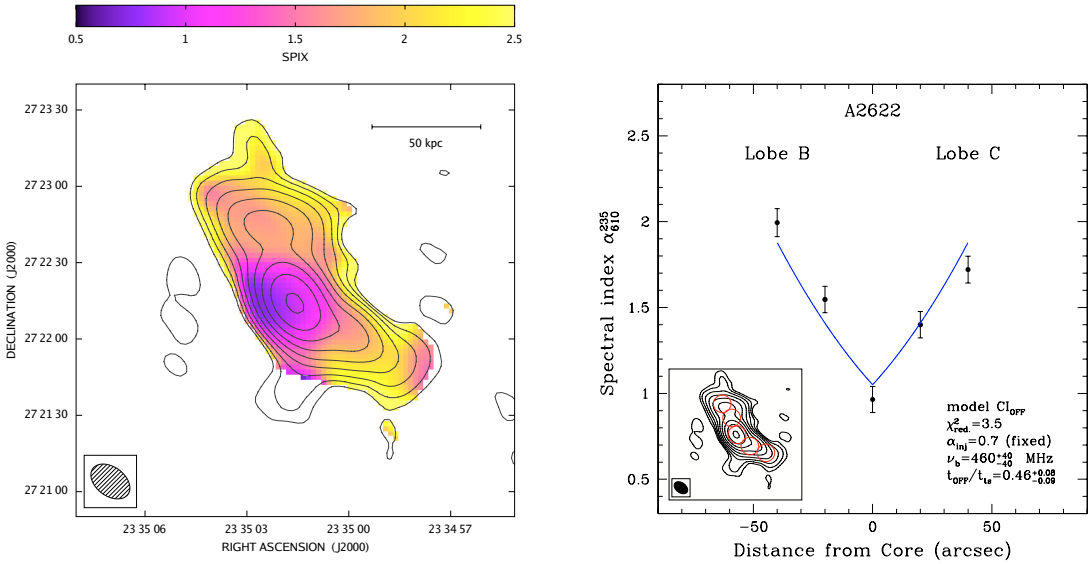

Fig. 24. A 2622 – *Left*: colour scale image of the spectral index distribution between 235 MHz and 610 MHz over central radio galaxy, as computed from images with a restoring beam of 17.1″ × 11.4″. Overlaid are the GMRT 610 MHz logarithmic contours starting from 0.3 mJy. *Right*: 235 MHz−610 MHz spectral index distribution of the lobes as function of the distance from the core. The solid line is the best fit of the radiative model described in the text.

Given the total size of the source, we obtained a projected expansion velocity of ∼5000 km s^{-1} for each lobe (∼0.02c).

5.6. A 2622. Spectral analysis along the lobes

The image of the 235 MHz–610 MHz spectral index distribution over the source is reported in the left panel of Fig. 24.

The region with the flattest spectral index ($\alpha \sim 0.7$) is not coincident with the peak brightness at either frequency. Outside this region the spectrum steepens considerably along the lobes, reaching values $\alpha \gtrsim 2$. Such an offset between the 235 MHz−610 MHz spectral index image and the peak in the total intensity is intriguing. One possible interpretation is that this radio galaxy is old, and the flattest region reveals the original location of the nucleus.

The hypothesis of an old radio source, whose nuclear engine might be switched off, is supported by the analysis of the integrated spectrum between 80 MHz and 4.5 GHz, shown in Fig. 25. Open circles are literature data and filled circles are the GMRT data given in Table 4. Also for this source our observations are consistent with the flux density measurements known from the literature. The spectrum can be fitted with a single power law over the whole range 80 MHz−4.5 GHz, with a spectral index of $\alpha = 1.7$. The solid line in the figure represents the best fit of the CI model to the integrated spectrum, which provides $\alpha_{\rm inj} = 1.1^{+0.0}_{-0.1}$.

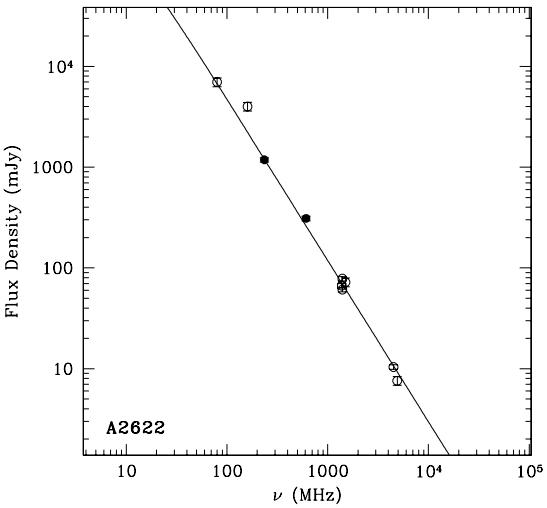

Fig. 25. A 2622 – Radio spectrum of the central radio galaxy between 80 MHz and 4.5 GHz. The empty circles are literature data, filled circles are the 235 MHz and 610 MHz measurements. The solid line is the best fit of the CI model.

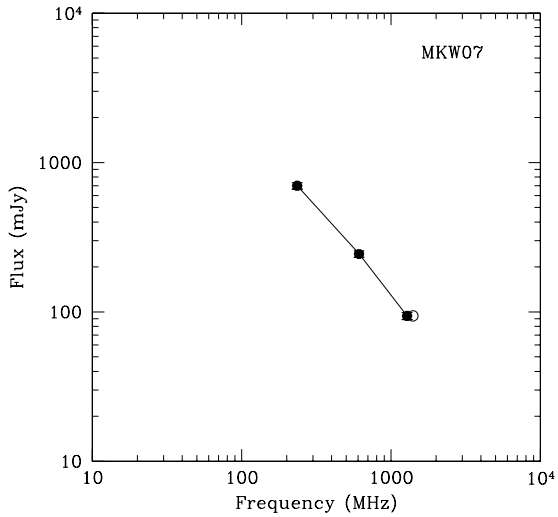

Fig. 26. MKW 07 – Radio spectrum of the central radio galaxy between 235 MHz and 1.4 GHz. The filled circles are the GMRT data; the empty circle is the NVSS value at 1.4 GHz.

For this source we managed to carry out the analysis of the spectral distribution along the lobes. We derived the trend of the spectral index between 235 MHz and 610 MHz in the source lobes (B and C in Fig. 10 and right panel of Fig. 24) as a function of the distance from the peak, and fitted the observed steepening. The spectrum is very steep everywhere along the lobes. The "flattest" value of the spectral index is ∼1.1, then it further steepens (up to ∼2) with increasing distance from the core along both lobes.

The overall spectral properties of the source suggest that it is most likely switched off. For this reason we fitted the spectra along the lobes assuming an initial phase of electron injection, followed by a switch-off of the nuclear activity and then a "relic" phase (Parma et al. 2007). An isotropic distribution of the pitch angle (JP model; Jaffe & Perola 1974) is assumed.

We imposed an initial spectral index $\alpha_{\rm inj} = 0.7$, which provides a break frequency $\nu_{\rm b} = 460^{+40}_{-40}$ MHz, $B_{\rm eq} = 4.4$ μG, and a total source age $t_{\rm rad} = 1.5 \times 10^8$ yr. Furthermore, we obtained that $t_{\rm off}/t_{\rm rad} = 0.46$, where $t_{\rm off}$ is the duration of the switched–off phase (see Parma et al. 2007 for details). This means that the source has been active for 79 Myr and switched off 67 Myr ago.

5.7. MKW 07. Spectral properties

The total integrated synchrotron spectrum of the source between 235 MHz and 1.28 GHz is shown in Fig. 26. The source spectrum is steep in this frequency range, with a spectral index $\alpha^{1.28\ \rm GHz}_{235\ \rm MHz} = 1.2 \pm 0.1$. No information was found in the literature at other frequencies, therefore no detailed study of the integrated spectrum was possible.

We produced an image of the spectral index distribution over the source between 235 MHz and 1.28 GHz, which is shown in Fig. 27. There is no obvious trend of the spectral index in both lobes. The distribution is patchy, with $\alpha^{1.28\ \rm GHz}_{235\ \rm MHz}$ in the range ∼1 ÷ 1.5, suggesting that the lobes are old structures expanding adiabatically.

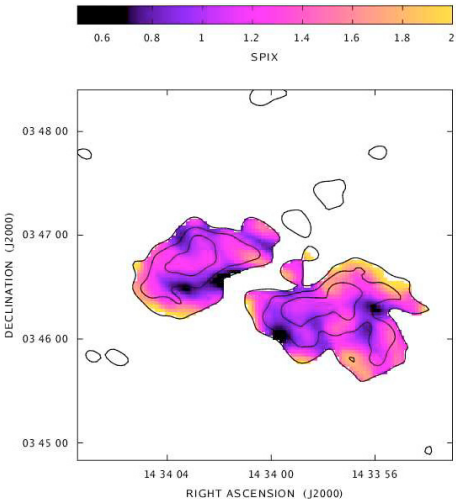

Fig. 27. MKW 07 – Colour scale image of the spectral index distribution between 235 MHz and 1.28 GHz over the central radio source, as computed from images with a restoring beam of 14.0″ × 9.1″. Overlaid are the GMRT 235 MHz contours at levels 4.5, 9, 18, 36, 72, 144, 288 mJy.

5.8. MKW 03s. Study of the integrated spectrum

The radio galaxy at the centre of MKW 03s is a well-known ultra steep spectrum radio galaxy (3C 318.1; e.g. Komissarov & Gubanov 1994; de Breuck et al. 2000) and flux density measurements are available from 16.7 MHz up to 4.9 GHz. We collected these values and plotted them in Fig. 28, together with our GMRT observations, to derive the source total synchrotron spectrum. Also for this radio galaxy our GMRT flux densities align extremely well with the literature data. The average spectral index for this source is $\alpha \sim 1.9$.

The ultra-steep integrated spectrum of this source cannot be explained by a simple CI model. It is likely that the injection of electrons in the source has stopped. However, the high-frequency cutoff of the synchrotron spectrum is less than exponential. A possible explanation is that the relic electrons are ageing in a filamentary magnetic field and that their diffusion is very low. Under these conditions, different parts of the source would have slightly different break frequencies and this

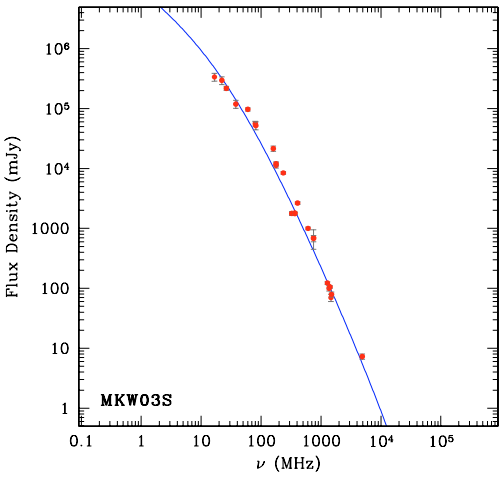

Fig. 28. MKW 03s – Radio spectrum of the central radio galaxy between 16.7 MHz and 1.47 GHz. The empty circles are literature data, the filled circle are the GMRT data at 235 MHz, 610 MHz and 1.28 GHz. The solid line is the best fit of the MJP model.

would cause a smoother cutoff of the intregrated spectrum. For this source we indeed obtained a very good fit of the spectrum between 16.7 MHz−4.9 GHz (solid line in Fig. 28) using a diffusion MJP model (Slee et al. 2001), which accounts for the effects of particle diffusion in an inhomogeneous magnetic field whose intensity is spatially variable. The model includes an initial phase of electron injection (CI), followed by a switch-off of the nuclear activity and then a "relic" phase. An isotropic distribution of the pitch angle (JP model; Jaffe & Perola 1973) is assumed. We fixed the injection spectral index of the CI phase to $\alpha_{\rm inj} = 0.7$, and obtained a best fit value of the break frequency $\nu_{\rm b} = 30 \pm 1$ MHz (Table 6). The model provides a ratio $B_{\rm rms}/B_{\rm CMB} = 16^{+18}_{-6}$. Since for this source $B_{\rm CMB} = 3.5\ \mu$G, we have $B_{\rm rms} = 56\ \mu$G, and the corresponding radiative age (see Formula 2) is $t_{\rm rad} = 2.1 \times 10^7$ yr. We were also able to estimate the relative duration of the relic phase $t_{\rm off}$ with respect to the CI phase $t_{\rm rad}$: $t_{\rm off}/t_{\rm rad} > 0.46$, i.e. the CI phase lasted about $\sim 1.1 \times 10^7$ yr and the nuclear engine switched off at least $\sim 10^7$ yr ago.

For this source the equipartition magnetic field is $B_{\rm eq} \sim 16\ \mu$G. This value and the overall size of MWK 03s are very similar to what is found for the dying sources in Parma et al. (2007).

6. Discussion

6.1. Radio powers and morphologies

In this paper we presented new GMRT images at 1.28 GHz, 610 MHz and 235 MHz for 13 cD galaxies selected from a statistical sample of rich and poor galaxy clusters located at $z \leq 0.1$. Both the radio power range and the variety of morphologies found are typical for radio galaxies at cluster centres. It is well known (i.e. Valentjin & Bijleveld 1983; Ball et al. 1993; Burns et al. 1987; Bagchi & Kapahi 1994) that the radio emission associated with cD galaxies exhibits a large variety of morphologies, regardless of the cluster richness: compact radio sources, classical doubles with FR I and FRI/FRII morphology, wide-angle-tails (WAT; e.g. 3C 465 in A 2634, Eilek & Owen 2002), core-halo (e.g. 3C 84 in the Perseus cluster, Fabian et al. 2000), and more peculiar structures, for example the complex radio source associated with the cD galaxy in A 3560 (Bardelli et al. 2002) and that in A 2199 (3C 338, Giovannini et al. 1998).

Here we give a brief summary.

i) All sources are low/intermediate power radio galaxies, as typically found in the innermost cluster regions. Their radio power at 1.4 GHz (Table 1) ranges from $\log P_{1.4\ \rm GHz}$ (W Hz^{-1}) = 21.86 (MKW 01s) to $\log P_{1.4\ \rm GHz}$ (W Hz^{-1}) = 24.66 (A 2480).
ii) We found two sources with a galactic size and morphology typical of FR Is (A 1663) and FR I/II (A 2480); a point-like source associated with the nucleus of the cD galaxy in the poor cluster MKW 01s, whose origin is unclear and could be due both to a very faint AGN or to nuclear starburst; a core-halo source in MKW 01; a double radio source in AWM 05, with a strong nuclear component. Finally, a weak AGN with faint lobes was found in MKW 06.
iii) Three sources, A 2162, MKW 07 and MKW 03s, show a fairly relaxed morphology of the lobes and lack nuclear emission. These features are consistent with the idea that they are aged radio galaxies, as also suggested by the results of the spectral analysis (see Sects. 5.4, 5.7, 5.8 and 6.3).
iv) The sample includes three very extended radio galaxies, including the cluster-size double radio galaxy in A 2372, whose lobes are most likely undergoing strong interaction with the ICM; the double source at the centre of MKW 02, whose images at these two frequencies show only the central component and the brightest regions in the lobes; the dumbbell system in A 1775, characterised by a galactic size double source and a spectacular head-tail source, extending out to ∼380 kpc.

In the following subsections we will present a few general considerations on the spectral properties and radiative ages for these sources, in the light of the extreme environment in which they are hosted.

6.2. Steepness of the radio spectrum

It is well known from the literature that the spectra of radio galaxies in central cluster regions tend to be steeper than in other environments (i.e. Slee et al. 1983; Slee & Reynolds 1984; Roland et al. 1985; Slee et al. 2001), with $\alpha > 1$ and up to the ultra steep values reported in de Breuck et al. (2000). This has been explained in terms of confinement of the ICM of the radio emitting plasma; the confined relativistic plasma loses its high energy electrons through synchrotron and Inverse Compton losses, resulting in a steepening of the radio spectrum.

The analysis of the spectral index for the sources presented here shows that also in our sample most of the sources have steep spectrum. From Tables 4−6 we can say that 3/13 sources have a "normal" spectrum, with α ranging from 0.7 to 0.8. Among these sources, we draw the attention to A 2480. The source is peculiar in many ways, since it is one of the smallest in the sample, the most powerful, and on the basis of the spectral analysis it is also the youngest.

Among all the remaining sources, the largest majority (10/13), have observed spectra steeper than 1, up to the ultra steep spectrum of MKW 03s and A 2622.

6.3. Source ages. Active and "dying" radio galaxies

Table 6 shows that 4 out of the 7 sources with available estimates of their radiative age have $t_{\rm rad} \gtrsim 10^8$ yr. Such ages are of the same order of magnitude found for giant radio galaxies. There are a few exceptions worth to be mentioned.

A 2622 and MKW 03s are most likely "dying" sources, where the nuclear engine has switched off and the spectrum is dominated by synchrotron and Inverse Compton losses. In both cases, the radiative model that better describes the source spectrum requires a switch-off of the central engine, followed by a "relic" phase, and this allowed us to estimate the ratio $t_{\rm off}/t_{\rm rad}$. The radiative age is of the order of a few Myr for both sources.

For all the remaining steep spectrum sources, there is evidence of nuclear emission with a flattish spectrum: the head of the tail in A 1775 (Fig. 20) has an average spectrum of ∼0.5; the central component in MKW 02 has a spectral index of 0.5 (Table 4).

MKW 07 (Fig. 12) is an intriguing source. Compact emission is associated with the western optical nucleus in the galaxy, but the bulk of the radio emission comes from two lobes with a steep spectrum. The measurement of the flux density of the compact component is difficult at 610 MHz and 235 MHz, since it is blended with the emission from the south-western lobe, and it is most likely overestimated. For this reason the spectral index given in Table 4 for this component is very uncertain. The radio-optical overlay in the image is reminiscent of 3C 338, which is thought to be the superposition of old emission and restarted nuclear activity. Here at 1.28 GHz and at 610 MHz the two lobes are clearly connected with a ridge of emission superposed on the eastern nucleus. A possible interpretation of this peculiar source is that the two lobes are associated with a past cycle of radio activity associated with the eastern nucleus.

Table 6 reports a crude estimate of the source growth velocity, based on the radiative ages estimated from the analysis of the integrated spectrum and from the total source size (end to end). These values are considerably smaller than the typical expansion velocities estimated for the large radio galaxies, due to the combination of the high radiative ages found and the relatively small/average sizes of the radio galaxies (except A 2372 and the tail in A 1775). It is tempting to relate these values to the dense environment at the centres of galaxy clusters, causing a slow growth rate. The growth velocity estimated for A 2480 would fit this idea, since it is a young source still embedded in the optical host. Unfortunately, high resolution X-ray data are unavailable for all sources presented here, and this does not allow us to derive the properties of the external medium and check whether they are overpressured, and/or highly confined.

The radiative ages estimated here are all based on the assumption that the spectral steepening is due to particle ageing in a constant magnetic field. Alternative models have been developed for classical double radio galaxies, which consider the role of a decreasing magnetic field along the strucure of extended radio galaxies (e.g. Blundell & Rawlings 2000, and references therein). Such a configuration of the magnetic field would also reflect in a spectral steepening, with no direct implication for the source ageing. However, the radio sources in our sample are significantly weaker than the classical FRII type sources. In particular, the magnetic field strength in the sources of our sample is of the same order as the equivalent magnetic field associated with the inverse Compton losses $B \sim B_{\rm IC}$. This implies a scaling for the break frequency of $\nu_{\rm b} \propto B t_{\rm rad}^{-2}$ (see Eq. (1)) rather than $\nu_{\rm b} \propto B^{-3} t_{\rm rad}^{-2}$, as expected in the case of powerful radio sources where $B \gg B_{\rm IC}$. Consequently, in the low power sources considered in this work, the observed spectral steepening should be less sensitive to systematic variations of magnetic field strength. Although these variations should have a low impact on the spectral steepening, we cannot completely rule out their effects and thus our age estimates should be considered upper limits, and the computed velocity growth as lower limits.

6.4. A 2372: a restarted radio galaxy?

The WAT in A 2372 is unique in many ways. Beyond the very large angular extent, the gap of radio emission visible between the inner jets of A 2372 (coincident with the optical galaxy) and the large scale lobes (see Fig. 9) may contain very relevant information. This feature appears also in higher frequency images available in the literature (1.4 GHz, Owen & Ledlow 1997; 4.9 GHz, Gregorini et al. 1994). Such a large gap is uncommon in low power radio galaxies, and suggests that this galaxy might be undergoing intermittent activity of the radio nucleus. The double morphology of the nuclear component (insert in the upper panel of Fig. 9) is a clear indication that the radio nucleus is currently active.

The emission gap is ∼40 kpc (from the galaxy to the edge of the lobes). Using the source LLS (Table 4) and its radiative age (Table 6), we made a first order estimate of the growth velocity of this source, and obtained $v_{\rm growth} \sim {\rm LLS}/t_{\rm rad} \sim 0.03{\rm c}$. These numbers allow us to make a rough estimate of the time elapsed since the last refuelling of the radio lobes, i.e. $t_{\rm gap} \sim 10^6$ yr.

We suggest therefore that this radio galaxy might be characterised by intermittent activity of the radio nucleus, on a time scale which is ∼1/100 of the total lifetime of the source. If confirmed, this would be the first case of a direct measurement of a cycle of activity in a radio galaxy.

One possible way to check for further hints of recurrent activity is to study the properties of the intracluster medium with high sensitivity and resolution, to search for bubbles and/or temperature gradients. A similar study was carried out for the cluster 2A 0335+096 by Mazzotta et al. (2003) who estimated expected bursts of radio activity with cycles of the order of 10^7 years. However, such a study is not possible for A 2372 with the current generation of X-ray satellites. Ledlow et al. (2003) report a ROSAT (0.2−2 keV) luminosity $L_{\rm X} = 2.2 \times 10^{42}$ erg/s, with an observed flux $f_{\rm X} = 0.22 \times 10^{-12}$ erg cm^{-2} s−1. This cluster is therefore too faint to detect cavities with some significance.

7. Summary and conclusions

In this paper we presented high resolution and high sensitivity GMRT radio images for 13 radio galaxies located at the centres of rich galaxy clusters and poor groups, and carried out a morphological and spectral analysis.

Our deep images revealed a variety of morphologies, i.e. compact, double and tailed sources, and linear sizes ranging from the sub-kpc scale to almost the Mpc scale. No difference in the morphology and size was found among cluster and group cD galaxies.

On the basis of our observations and literature data, we derived steep spectra ($\alpha \geq 1$ in the range ∼0.2−1.4 GHz) for 10/13 radio galaxies, confirming the known result that the central regions of clusters tend to host steep radio sources.

For 7 sources in the sample we could carry out a detailed spectral analysis, which allowed us to estimate the equipartition parameters and source radiative ages. We found radiative ages in the range $\sim 1.5 \times 10^7 \div \sim 5 \times 10^8$ yr. These ages, coupled with the linear sizes measured from our images, provide growth velocities considerably lower than what is found in the literature for the velocity advance speed of double radio galaxies. There seems to be no connection between the growth velocity and the large scale environment (i.e. no difference between rich and poor clusters).

Our analysis suggests that A 2622 and MKW 03s might be "dying" radio galaxies, where the nucleus has switched off and

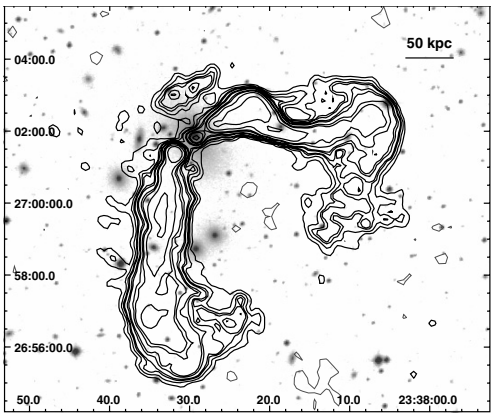

Fig. A.1. GMRT 235 MHz radio contours of the central WAT radio galaxy in A 2634, overlaid on the POSS–2 optical image. The 1σ level in the image is 1 mJy b^{-1}. Logarithmic contours are reported, starting from ± 5 mJy b^{-1}. The contour peak flux is 808 mJy b^{-1}. The *HPWB* is $17.1'' \times 11.4''$, PA 53°. The image is corrected for the primary beam of the GMRT antenna at 235 MHz.

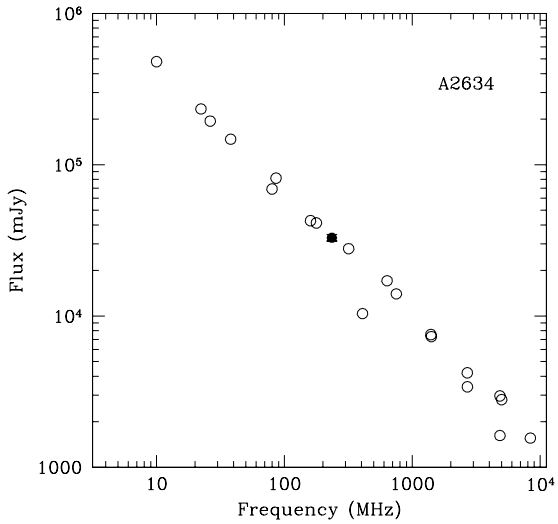

Fig. A.2. Radio spectrum of the central radio galaxy in A 2634 between 10 MHz and 8.4 GHz. The empty circles are literature data, the filled circle is the GMRT flux density of the source at 235 MHz.

the lobes are not currently fed by an active nucleus. The overall properties of MKW 03s (age, size, magnetic field strength) are very similar to those reported by Parma et al. (2007) for the dying source in their sample.

A 2372 has aged lobes and an active nucleus, and might represent a clear example of a restarted radio galaxy. For this source we estimated a life cycle of the order of 10^6 yr.

Acknowledgements. We thank the staff of the GMRT for their help during the observations. GMRT is run by the National Centre for Radio Astrophysics of the Tata Institute of Fundamental Research. S.G. and T.V. acknowledge partial support from the Italian Ministry of Foreing Affairs. This research has made use of the NASA/IPAC Extragalactic Database (NED) which is operated by the Jet Propulsion Laboratory, California Institute of Technology. The authors made use of the database CATS of the Special Astrophysical Observatory (Russia). Funding for the SDSS and SDSS-II has been provided by the Alfred P. Sloan Foundation, the Participating Institutions, the National Science Foundation, the US Department of Energy, the National Aeronautics and Space Administration, the Japanese Monbukagakusho, the Max Planck Society, and the Higher Education Funding Council for England. The SDSS Web Site is `http://www.sdss.org/`. The SDSS is managed by the Astrophysical Research Consortium for the Participating Institutions.

Appendix A: Abell 2634 (3C 465)

In this Appendix we present the GMRT 235 MHz image of the central cD galaxy in A 2634 ($z = 0.029$). This cluster belongs to our complete sample of cD galaxies, selected as described in Sect. 2. Due to the amount of radio information available in the literature, A 2634 was not selected for the GMRT observations presented in this paper. However the cluster is located within the field of view of the GMRT 235 MHz observation of A 2622, presented in Sect. 4.2. In particular A 2634 is ∼50′ south-east of A 2622, and thus within the 108′ radius primary beam of the GMRT antenna at 235 MHz. This is the first radio image of 3C 465 ever published at this radio frequency.

The radio source 3C 465, associated with the cD galaxy in A 2634 is considered the prototype of WAT sources. It has been studied in detail both in the radio (e.g. Eilek & Owen 2002; Hardcastle & Sakelliou 2004 and references therein) and X-ray band (Hardcastle et al. 2005).

The full resolution 235 MHz image of 3C 465 (corrected for the primary beam of the GMRT antenna at 235 MHz) is shown in Fig. A.1. Its total flux density is $S_{235\ \mathrm{MHz}} = 32.9$ Jy, and the derived radio power is $\log P_{235\ \mathrm{MHz}}$ (W Hz^{-1}) = 25.84. At this frequency and resolution 3C 465 exhibits some interesting features. A ridge is visible north of the western jet, with no obvious associated optical counterparts (at the magnitude limit of the POSS–2 image). Hints of this feature are visible also at 74 MHz on the VLSS, and for this reason we tend to rule out the possibility that it is an artifact of our image. The radio jets are very well confined all the way to the outermost edges, then they spread out in two converging tails, again in agreement with the VLSS.

In Fig. A.2 we show the integrated synchrotron spectrum of the source, determined using the flux density measured from our 235 MHz image and the literature data. The GMRT 235 MHZ flux density perfectly aligns with all the spectral data.

References

Abell, G. O., Corwin, H. G., & Olowin, R. P. 1989, ApJSS, 70, 1
Albert, C. E., White, R. A., & Morgan, W. W. 1977, ApJ, 211, 309
Bagchi, J., & Kapahi, V. K. 1994, JApA, 15, 275
Ball, R., Burns, J. O., & Loken, C. 1993, AJ, 105, 53
Bardelli, S., Venturi, T., Zucca, E., et al. 2002, A&A, 396, 65
Baum, S. A., & O'Dea, C. P. 1991, MNRAS, 250, 737
Becker, R. H., White, R. L., & Helfand, D. J. 1995, ApJ, 450, 559
Blanton, E. L. 2004, Proceedings of The Riddle of Cooling Flows in Galaxies and Clusters of Galaxies, ed. T. Reiprich, J. Kempner, & N. Soker, 181
Blanton, E. L., Sarazin, C. L., McNamara, B. R., & Wise, M. W. 2001, ApJ, 558, L15
Blundell, K. M., & Rawlings, S. 2000, AJ, 119, 1111
Böhringer, H., Schuecker, P., Pratt, G. W., & Finoguenov, A. 2007, Proceedings of Heating vs. Cooling in Galaxies and Clusters of Galaxies, ESO Astrophysics Symposia (Springer-Verlag)
de Breuck, C., van Breugel, W., Röttgering, H. J. A., & Miley, G. 2000, A&AS, 143, 303
Brunetti, G., Setti, G., & Comastri, A. 1997, A&A, 325, 898
Burns, J. O., Hanisch, R. J., White, R. A., et al. 1987, AJ, 94, 587
Condon, J. J., Cotton, W. D., Greisen, E. W., et al. 1998, AJ, 115, 1693
Dressel, L. L., & Condon, J. J. 1978, ApJS, 36, 53
Eilek, J. A., & Owen, F. N. 2002, ApJ, 567, 202
Fabian, A. C., Sanders, J. S., Ettori, S., et al. 2000, MNRAS, 318, L65
Fanaroff, B. L., & Riley, J. M. 1974, MNRAS, 167, 31
Giacintucci, S., Mazzotta, P., Brunetti, G., et al. 2006, AN, 327, 573
Giovannini, G., Cotton, W. D., Feretti, L., et al. 1998, ApJ, 493, 632
Gregorini, L., de Ruiter, H. R., Parma, P., et al. 1994, A&AS, 106, 1
Hardcastle, M. J., & Sakelliou, I. 2004, MNRAS, 349, 560
Hardcastle, M. J., Sakelliou, I., & Worall, D. M. 2005, MNRAS, 359, 1007
Jaffe, W. J., & Perola, G. C. 1974, A&A, 26, 423

Jones, C., Mandel, E., Schwarz, J., et al. 1979, ApJ, 234, L21
Kardashev, N. S. 1962, SvA, 6, 317
Komissarov, S. S., & Gubanov, A. G. 1994, A&A, 285, 27
Lara, L., Marquez, I., Cotton, W. D., et al. 1999, A&A, 348, 699
Jones, C., & Forman, W. 1999, ApJ, 511, 65
Ledlow, M. J., Owen, F. N., & Eilek, J. A. 2002, NewAR, 46, 343
Ledlow, M. J., Voges, W., Owen, F. N., & Burns, J. O. 2003, AJ, 126, 2740
Mathews, T., Morgan, W., & Schmidt, M. 1964, ApJ, 140, 35
Mazzotta, P., Edge, A. C., & Markevitch, M. 2003, ApJ, 596, 190
Mazzotta, P., Brunetti, G., Giacintucci, S., et al. 2004, JKAS, 37, 381
McNamara, B. R., Wise, M., Nulsen, P. E. J, et al. 2000, ApJ, 534, L135
McNamara, B. R., Wise, M. W., Nulsen, P. E. J., et al. 2001, ApJ, 562, L149
Merritt, D., & Ferrarese, L. 2001, MNRAS, 320, L30
Morgan, W. W., Kayser, S., & White, R. A. 1975, ApJ, 199, 545
Murgia, M. 2001, Ph.D. Thesis, University of Bologna
Owen, F. N., & Ledlow, M. J. 1997, ApJS, 108, 41O
Parma, P., Cameron, R. A., & De Ruiter, H. R. 1991, AJ, 102, 1960
Parma, P., Murgia, M., Morganti, R., et al. 1999, A&A, 344, 7
Parma, P., Murgia, M., de Ruiter, H. R., & Fanti, R. 2002, New Astr. Rev., 46, 313
Parma, P., Murgia, M., de Ruiter, H. R., et al. 2007, A&A, 470, 875
Roland, J., Hanish, R. J., Veron, P., & Fomalont, E. 1985, A&A, 148, 323
Sarazin, C. L., Baum, S. A., & O'Dea, C. P. 1995, ApJ, 451, 125
Schoenmakers, A. P., de Bruyn, A. G., Röttgering, H. J. A., et al. 2000, MNRAS, 315, 371
Slee, O. B., & Reynolds, J. E. 1984, PASA, 5(4), 516
Slee, O. B., Siegman, C. B., & Wilson, I. R. G. 1983, AuJPh, 36, 101
Slee, O. B., Roy, A. L., Murgia, M., et al. 2001, AJ, 122, 1172
Struble, M. F., & Rood, H. J. 1987, ApJS, 63, 555
Valentjin, E. A., & Bijleveld, W. 1983, A&A, 125, 223
Van den Bergh, S. 1977, PASP, 89, 746
Venturi, T., Dallacasa, D., & Stefanachi, F. 2004, A&A, 422, 515
Verkhodanov, O. V., Trushkin, S. A., Andernach, H., & Cherenkov, V. N. 1997, ASP Conf. Ser., 125, 322
de Young, A. 2004, Ph.D. Thesis, University of Minnesota